degrees, FOV = 16 × 16 × 0.5. A total of 29 high-resolution coronal slices of the whole brain were collected. Total scanning time was 60 min per individual. Within the 29 MRI slices, 8 slices contained the hippocampal formation (from bregma −0.90 to −4.40), which was manually selected by the paintbrush tool and used for the volumetric calculation of hippocampus using InsightITK-Snap software version 2.2.0.

Statistical Analysis

Data were analyzed by Student's t test if not stated otherwise and are presented as average ± SEM.

SUPPLEMENTAL INFORMATION

Supplemental Information includes four figures and one table and can be found with this article online at http://dx.doi.org/10.1016/j.celrep.2013.08.042.

ACKNOWLEDGMENTS

We thank Keiji Tanaka and Shigeyoshi Itohara for generously providing *Atg7*$^{flox/flox}$ and CamKII-*Cre* mice, respectively. We acknowledge the members of the PNS lab, Jiro Takano, Ko Sato, Kenichi Nagata, Naomasa Kakiya, Shoko Hashimoto, Hayato Isshiki, Kaori Tsukakoshi, Karin Sörgjerd, Emi Hosoki, Ryo Fujioka, Naomi Yamazaki, Yuya Tomita, and Yukiko Nagai. We appreciate the kind gift of the HDAC6 antibody from Tso-Pang Yao. This project was financially supported by research grants from Swedish Research Council, Sweden; RIKEN Brain Science Institute; Ministry of Education, Sports, Science and Technology, Japan; and Ministry of Health, Labour and Welfare, Japan.

Received: November 9, 2012
Revised: July 17, 2013
Accepted: August 23, 2013
Published: October 3, 2013

REFERENCES

Boland, B., Kumar, A., Lee, S., Platt, F.M., Wegiel, J., Yu, W.H., and Nixon, R.A. (2008). Autophagy induction and autophagosome clearance in neurons: relationship to autophagic pathology in Alzheimer's disease. J. Neurosci. *28*, 6926–6937.

Boland, B., Smith, D.A., Mooney, D., Jung, S.S., Walsh, D.M., and Platt, F.M. (2010). Macroautophagy is not directly involved in the metabolism of amyloid precursor protein. J. Biol. Chem. *285*, 37415–37426.

Caccamo, A., Majumder, S., Richardson, A., Strong, R., and Oddo, S. (2010). Molecular interplay between mammalian target of rapamycin (mTOR), amyloid-β, and Tau: effects on cognitive impairments. J. Biol. Chem. *285*, 13107–13120.

Deretic, V., Jiang, S., and Dupont, N. (2012). Autophagy intersections with conventional and unconventional secretion in tissue development, remodeling and inflammation. Trends Cell Biol. *22*, 397–406.

Hama, E., Shirotani, K., Masumoto, H., Sekine-Aizawa, Y., Aizawa, H., and Saido, T.C. (2001). Clearance of extracellular and cell-associated amyloid β peptide through viral expression of neprilysin in primary neurons. J. Biochem. *130*, 721–726.

Hamasaki, M., Furuta, N., Matsuda, A., Nezu, A., Yamamoto, A., Fujita, N., Oomori, H., Noda, T., Haraguchi, T., Hiraoka, Y., et al. (2013). Autophagosomes form at ER-mitochondria contact sites. Nature *495*, 389–393.

Hara, T., Nakamura, K., Matsui, M., Yamamoto, A., Nakahara, Y., Suzuki-Migishima, R., Yokoyama, M., Mishima, K., Saito, I., Okano, H., and Mizushima, N. (2006). Suppression of basal autophagy in neural cells causes neurodegenerative disease in mice. Nature *441*, 885–889.

Harris, H., and Rubinsztein, D.C. (2012). Control of autophagy as a therapy for neurodegenerative disease. Nat. Rev. Neurol. *8*, 108–117.

Inoue, K., Rispoli, J., Kaphzan, H., Klann, E., Chen, E.I., Kim, J., Komatsu, M., and Abeliovich, A. (2012). Macroautophagy deficiency mediates age-dependent neurodegeneration through a phospho-tau pathway. Mol. Neurodegener. *7*, 48.

Iwata, N., Mizukami, H., Shirotani, K., Takaki, Y., Muramatsu, S.-i., Lu, B., Gerard, N.P., Gerard, C., Ozawa, K., and Saido, T.C. (2004). Presynaptic localization of neprilysin contributes to efficient clearance of amyloid-β peptide in mouse brain. J. Neurosci. *24*, 991–998.

Jaeger, P.A., Pickford, F., Sun, C.-H., Lucin, K.M., Masliah, E., and Wyss-Coray, T. (2010). Regulation of amyloid precursor protein processing by the Beclin 1 complex. PLoS ONE *5*, e11102.

Komatsu, M., Waguri, S., Ueno, T., Iwata, J., Murata, S., Tanida, I., Ezaki, J., Mizushima, N., Ohsumi, Y., Uchiyama, Y., et al. (2005). Impairment of starvation-induced and constitutive autophagy in Atg7-deficient mice. J. Cell Biol. *169*, 425–434.

Komatsu, M., Waguri, S., Chiba, T., Murata, S., Iwata, J.-i., Tanida, I., Ueno, T., Koike, M., Uchiyama, Y., Kominami, E., and Tanaka, K. (2006). Loss of autophagy in the central nervous system causes neurodegeneration in mice. Nature *441*, 880–884.

Komatsu, M., Wang, Q.J., Holstein, G.R., Friedrich, V.L., Jr., Iwata, J.-i., Kominami, E., Chait, B.T., Tanaka, K., and Yue, Z. (2007). Essential role for autophagy protein Atg7 in the maintenance of axonal homeostasis and the prevention of axonal degeneration. Proc. Natl. Acad. Sci. USA *104*, 14489–14494.

LaFerla, F.M., Green, K.N., and Oddo, S. (2007). Intracellular amyloid-beta in Alzheimer's disease. Nat. Rev. Neurosci. *8*, 499–509.

Lee, J.-H., Yu, W.H., Kumar, A., Lee, S., Mohan, P.S., Peterhoff, C.M., Wolfe, D.M., Martinez-Vicente, M., Massey, A.C., Sovak, G., et al. (2010a). Lysosomal proteolysis and autophagy require presenilin 1 and are disrupted by Alzheimer-related PS1 mutations. Cell *141*, 1146–1158.

Majumder, S., Richardson, A., Strong, R., and Oddo, S. (2011). Inducing autophagy by rapamycin before, but not after, the formation of plaques and tangles ameliorates cognitive deficits. PLoS ONE *6*, e25416.

Mizushima, N., and Komatsu, M. (2011). Autophagy: renovation of cells and tissues. Cell *147*, 728–741.

Nixon, R.A. (2007). Autophagy, amyloidogenesis and Alzheimer disease. J. Cell Sci. *120*, 4081–4091.

Pickford, F.M.E., Masliah, E., Britschgi, M., Lucin, K., Narasimhan, R., Jaeger, P.A., Small, S., Spencer, B., Rockenstein, E., Levine, B., and Wyss-Coray, T. (2008). The autophagy-related protein beclin 1 shows reduced expression in early Alzheimer disease and regulates amyloid β accumulation in mice. J. Clin. Invest. *118*, 2190–2199.

Saido, T.C., Yokota, M., Maruyama, K., Yamao-Harigaya, W., Tani, E., Ihara, Y., and Kawashima, S. (1994). Spatial resolution of the primary beta-amyloidogenic process induced in postischemic hippocampus. J. Biol. Chem. *269*, 15253–15257.

Sturchler-Pierrat, C., Abramowski, D., Duke, M., Wiederhold, K.-H., Mistl, C., Rothacher, S., Ledermann, B., Bürki, K., Frey, P., Paganetti, P.A., et al. (1997). Two amyloid precursor protein transgenic mouse models with Alzheimer disease-like pathology. Proc. Natl. Acad. Sci. USA *94*, 13287–13292.

Tsien, J.Z., Chen, D.F., Gerber, D., Tom, C., Mercer, E.H., Anderson, D.J., Mayford, M., Kandel, E.R., and Tonegawa, S. (1996). Subregion- and cell type-restricted gene knockout in mouse brain. Cell *87*, 1317–1326.

Wirths, O., and Bayer, T.A. (2012). Intraneuronal Aβ accumulation and neurodegeneration: lessons from transgenic models. Life Sci. *91*, 1148–1152. http://dx.doi.org/10.1016/j.lfs.2012.02.001.

Yang, D.-S., Stavrides, P., Mohan, P.S., Kaushik, S., Kumar, A., Ohno, M., Schmidt, S.D., Wesson, D., Bandyopadhyay, U., Jiang, Y., et al. (2011). Reversal of autophagy dysfunction in the TgCRND8 mouse model of Alzheimer's disease ameliorates amyloid pathologies and memory deficits. Brain *134*, 258–277.

Yu, W.H., Cuervo, A.M., Kumar, A., Peterhoff, C.M., Schmidt, S.D., Lee, J.-H., Mohan, P.S., Mercken, M., Farmery, M.R., Tjernberg, L.O., et al. (2005). Macroautophagy—a novel β-amyloid peptide-generating pathway activated in Alzheimer's disease. J. Cell Biol. *171*, 87–98.

Zheng, L., Terman, A., Hallbeck, M., Dehvari, N., Cowburn, R.F., Benedikz, E., Kågedal, K., Cedazo-Minguez, A., and Marcusson, J. (2011). Macroautophagy-generated increase of lysosomal amyloid β-protein mediates oxidant-induced apoptosis of cultured neuroblastoma cells. Autophagy *7*, 1528–1545.

Dan et al. Acta Neuropathologica Communications 2013, 1:54
http://www.actaneurocomms.org/content/1/1/54

ACTA NEUROPATHOLOGICA COMMUNICATIONS

RESEARCH Open Access

Extensive deamidation at asparagine residue 279 accounts for weak immunoreactivity of tau with RD4 antibody in Alzheimer's disease brain

Ayaho Dan[1,4], Muneaki Takahashi[1], Masami Masuda-Suzukake[1], Fuyuki Kametani[1], Takashi Nonaka[1], Hiromi Kondo[2], Haruhiko Akiyama[3], Takao Arai[4], David MA Mann[5], Yuko Saito[6], Hiroyuki Hatsuta[7], Shigeo Murayama[7] and Masato Hasegawa[1*]

Abstract

Background: Intracytoplasmic inclusions composed of filamentous tau proteins are defining characteristics of neurodegenerative tauopathies, but it remains unclear why different tau isoforms accumulate in different diseases and how they induce abnormal filamentous structures and pathologies. Two tau isoform-specific antibodies, RD3 and RD4, are widely used for immunohistochemical and biochemical studies of tau species in diseased brains.

Results: Here, we show that extensive irreversible post-translational deamidation takes place at asparagine residue 279 (N279) in the RD4 epitope of tau in Alzheimer's disease (AD), but not corticobasal degeneration (CBD) or progressive supranuclear palsy (PSP), and this modification abrogates the immunoreactivity to RD4. An antiserum raised against deamidated RD4 peptide specifically recognized 4R tau isoforms, regardless of deamidation, and strongly stained tau in AD brain. We also found that mutant tau with N279D substitution showed reduced ability to bind to microtubules and to promote microtubule assembly.

Conclusion: The biochemical and structural differences of tau in AD from that in 4R tauopathies found in this study may therefore have implications for prion-like propagation of tau.

Keywords: Alzheimer's disease, Tau, Deamidation, Aging, Microtubule

Background

Intracellular inclusions composed of filamentous tau proteins are defining characteristics of many neurodegenerative diseases, including Alzheimer's disease (AD), Pick's disease, corticobasal degeneration (CBD), and progressive supranuclear palsy (PSP). Tau is a microtubule-associated protein that stabilizes microtubules and promotes their assembly. In adult human brain, 6 tau isoforms are expressed as a result of mRNA splicing. They are divided into two groups, 3-repeat (3R) and 4-repeat (4R) tau isoforms, according to whether or not exon 10 is expressed. Tau pathologies show clear morphological differences among different diseases or disease types, and different tau isoforms are accumulated in the diseased brains, namely, 6 tau isoforms in AD, 3R tau isoforms in Pick's disease, and 4R tau isoforms in PSP and CBD [1,2]. In addition, tau in PSP and tau in CBD are biochemically distinguished by the banding pattern of the C-terminal fragments [3]. However, it remains unclear why different tau isoforms accumulate in different diseases and how they lead to the formation of abnormal filamentous structures and pathologies.

Isoform-specific tau antibodies are useful tools for immunohistochemical and biochemical studies of tau species in diseased brains. In particular, RD3 and RD4 [4], which are specific antibodies to 3R and 4R tau isoforms, respectively, have been widely used to investigate tau pathologies [5-7]. One of the present authors (M.H.) had found that the asparagine residue at position 279 (N279), located in the RD4 epitope, was detected mostly as aspartic acid owing to deamidation of asparagine when PHF-tau in AD brains was subjected to protein sequencing and LC/MS/

* Correspondence: hasegawa-ms@igakuken.or.jp
[1]Department of Neuropathology and Cell Biology, Tokyo Metropolitan Institute of Medical Science, Setagaya-ku, Tokyo 156-8506, Japan
Full list of author information is available at the end of the article

MS analysis after digestion with lysyl endopeptidase [8]. Here, we show that the irreversible post-translational deamidation takes place at N279 (N279D) in the RD4 epitope of tau in AD, but not CBD or PSP, and this modification abrogates the immunoreactivity to RD4. We raised an antiserum against RD4 peptide with N279D in rabbit, and showed that it specifically recognizes 4R tau isoforms regardless of deamidation and strongly stained tau in AD brain. We further show that mutant tau with N279D substitution has a reduced ability to bind to microtubules and to promote their assembly. These results have important implications for immunohistochemical and other studies aimed at understanding the molecular mechanisms of tau accumulation in AD and other tauopathies.

Results

Low immunoreactivities of tau in AD and tau deamidated at N279 to RD4

When Sarkosyl-insoluble fractions of tau from AD, PSP and CBD brains were analyzed by immunoblotting with T46 and RD4, we noticed a lower immunoreactivity of RD4 with abnormal tau in AD compared to that in both PSP and CBD (Figure 1a,b). T46, a monoclonal antibody to the C-terminal region of tau, strongly labeled triplet bands of phosphorylated full-length tau in AD together with smearing substances, and doublet bands together with C-terminal fragments of tau in CBD and PSP (Figure 1a). In contrast, RD4 (1:1000 dilution) stained tau in CBD and PSP relatively strongly, but barely stained the tau bands, and especially the smears, in AD (Figure 1b), though both RD4 and T46 labeled Sarkosyl-soluble tau in these brains (Figure 1c,d). These results suggested that there might be some modification in the RD4 epitope or its vicinity on tau in AD abrogating immunoreactivity. The low affinity of RD4 for tau in AD is consistent with the original report [4], which noted that the RD4 titer appeared to be considerably weaker than those of TP70 and RD3. To confirm that the asparagine residue at position 279 (N279) on tau was deamidated in AD, we performed LC/MS/MS analyses of tryptic peptides of Sarkosyl-insoluble tau prepared from AD brains. As shown in Figure 1e, almost all the VQIINK peptide

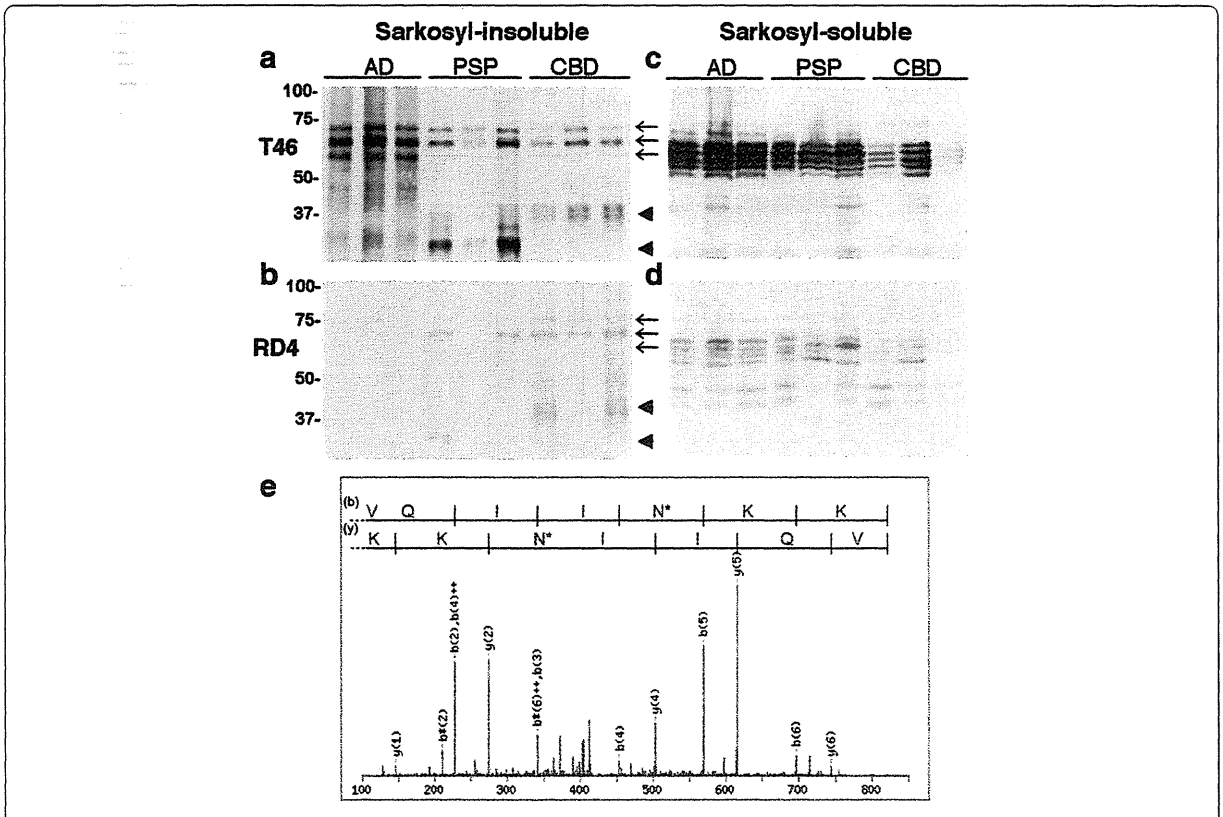

Figure 1 Immunoblot and LC/MS/MS analyses showed a lower immunoreactivity of RD4 with tau in AD and deamidation at N279. Immunoblot analysis of Sarkosyl-insoluble **(a, b)** and soluble **(c, d)** tau from AD, PSP and CBD brains (three cases for each disease) with anti-tau monoclonal antibodies T46 **(a, c)** and RD4 **(b, d)**. Arrows indicated the positions of the 60, 64, 68 kDa triplet tau bands in AD brains, and arrowheads indicate the ~33 and ~37 kDa C-terminal fragments that distinguish PSP and CBD. Identification of deamidated amino acid residue by nano-electrospray tandem mass spectrometry **(e)**. Product ion spectrum of a mass signal of tryptic peptide VQIINK detected in Sarkosyl-insoluble tau from AD brain, showing the b and y ion series. These results identify the site of deamidation as N279, indicated by N*.

derived from 4R tau isoform was detected as VQIIN*K (* indicates deamidation) (Figure 1e), while Q276 was normal, strongly suggesting that N279 is extensively deamidated in tau in AD.

RD4 cannot recognize 4R tau with deamidation at N279

Since N279 is located in the RD4 epitope, we next examined the effect of deamidation of N279 on immunoreactivity to RD4. Substitution of N279 to aspartic acid was introduced into 4R1N human tau isoform by site-directed mutagenesis, and immunoreactivity to mutant (N279D)-4R tau before and after phosphorylation by protein kinase A was compared with that of wild-type tau. As shown in Figure 2(a-d), RD4 was not able to recognize N279D-4R tau regardless of the phosphorylation state of Ser262, which is located near the RD4 epitope. To further investigate the

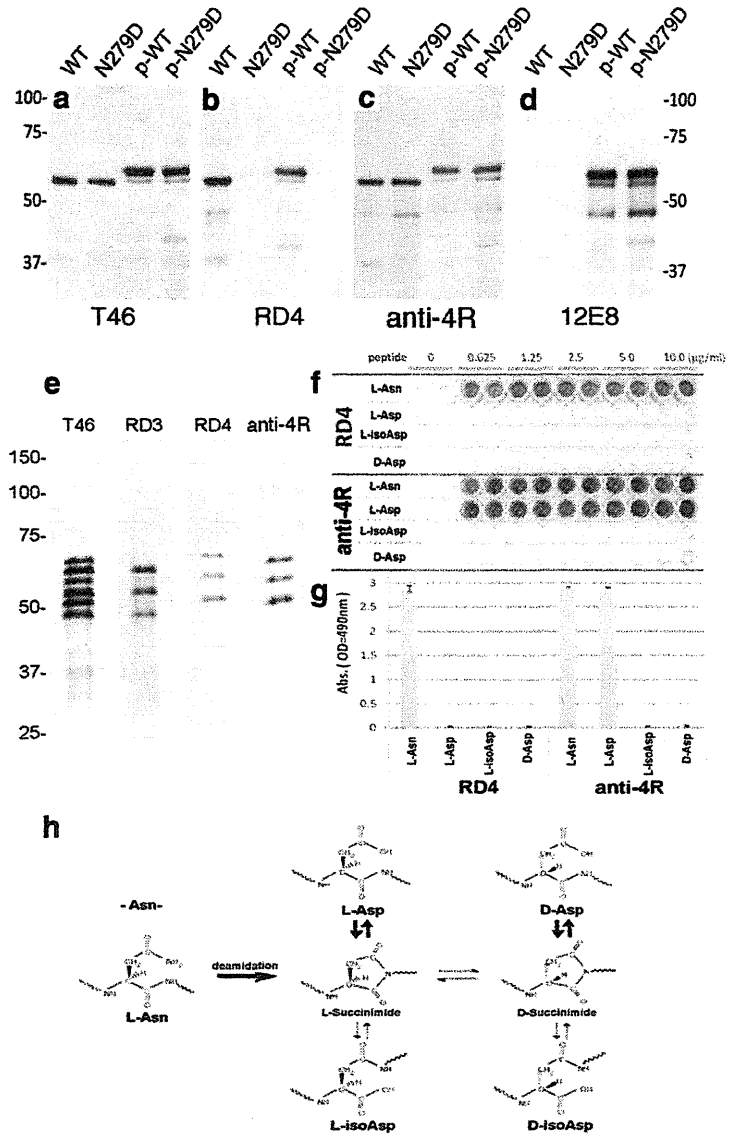

Figure 2 RD4 cannot recognize N279D-4R tau, but new anti-4R labels both WT and N279D-4R tau equally. Immunoblot analysis of wild-type (WT) and N279D mutant tau before (WT, N279D) and after (p-WT, p-N279D) phosphorylation with PKA, using T46 **(a)**, RD4 **(b)**, anti-4R **(c)** and 12E8 **(d)** antibodies. Immunoblot analysis of six recombinant human tau isoforms with T46, RD3, RD4 and anti-4R antibodies **(e)**. Specificities of RD4 (1:1000 dilutions) and anti-4R (1:3000 dilutions) antibodies for synthetic peptides, L-Asn (wild-type), L-Asp, L-isoAsp and D-Asp peptides (0.625 ~ 10 μg/mL) tested by ELISA assay **(f)**. Quantitation of the ELISA results (the mean of absorbance at 490 nm on 1.25 μg/mL peptide is shown **(g)**. Pathways for deamidation of asparaginyl residues **(h)**. L-Asn residue can be converted spontaneously via a succinimidyl intermediate to form L-Asp, D-Asp. L-isoAsp and D-isoAsp residue (modified from Ref. [9]).

deamidation of N279 of tau, we immunized a rabbit with a synthetic peptide, VQIIDKKLDLSNVQSKC, which is the RD4 antigen peptide with substitution of N279 to Asp. The antiserum anti-4R labeled both wild-type (WT) and N279D-4R tau equally (Figure 2c) and the immunoreactivity was unaffected by phosphorylation of Ser262/356 with PKA (Figure 2c). The anti-4R antibody specifically bound with recombinant human 4R tau isoforms, as did RD4, but did not react with the 3R tau isoforms (Figure 2e). The specificities of RD4 and anti-4R antibodies were further analyzed by means of ELISA assay using the antigen peptide of RD4 (L-Asn), the peptide with N279D substitution (L-Asp), the peptide with L-isoAsp substitution (L-isoAsp) and the peptide with N279 D-Asp substitution (D-Asp) (Figure 2f,g). These modifications are known to be related to deamidation of Asn residue (Figure 2h). RD4 failed to react with L-Asp (antigen peptide with N279D substitution), whereas anti-4R reacted almost equally with L-Asn (wild-type) and L-Asp peptide. Neither RD4 nor anti-4R reacted with D-Asp or L-isoAsp peptide (Figure 2f,g).

Antiserum against peptide with deamidation of N279 strongly stained tau smears in AD

The immunoreactivity of anti-4R was compared to that of RD4, RD3 and T46 in immunoblotting of Sarkosyl-insoluble tau from tauopathy brains (Figure 3). Samples of insoluble tau from three AD (lane 1–3), two PSP (lane 3, 4) and two CBD (lane 6, 7) cases were examined (Figure 3a-d). RD4 faintly stained only two bands at 64 and 68 kDa in AD brains, whereas it stained several tau fragments in PSP and CBD, in addition to the two bands at 64 and 68 (Figure 3b). In contrast, anti-4R stained tau bands and smears in AD, like RD3, and this staining was much stronger than that of tau bands and smears in PSP and CBD (Figure 3d). These results strongly suggest that tau in AD brains is predominantly deamidated at N279, and that the levels of deamidation are much lower in tau from PSP and CBD brains.

Next, we compared the immunostaining of tau pathologies with RD3, RD4 and anti-4R on formalin-fixed brain sections of AD (Figure 4). None of the three antibodies stained tau on formalin-fixed sections in the absence of formic acid treatment or autoclaving (not shown), suggesting that the epitopes of these antibodies are masked. After autoclaving or formic acid treatment, neurofibrillary tangles (NFTs) and neuropil threads (NTs) were detected with these antibodies, and dual treatment with both autoclaving and formic acid strongly enhanced the staining (not shown). The new anti-4R antibody stained intracellular NFTs and NTs more extensively than did RD4 (Figure 4). This was most evident in the CA1 region, where anti-4R strongly stained RD3+/RD4– NFTs (Figure 4d,f). This result indicates that the RD4 epitope is deamidated in pathological tau from AD brain,

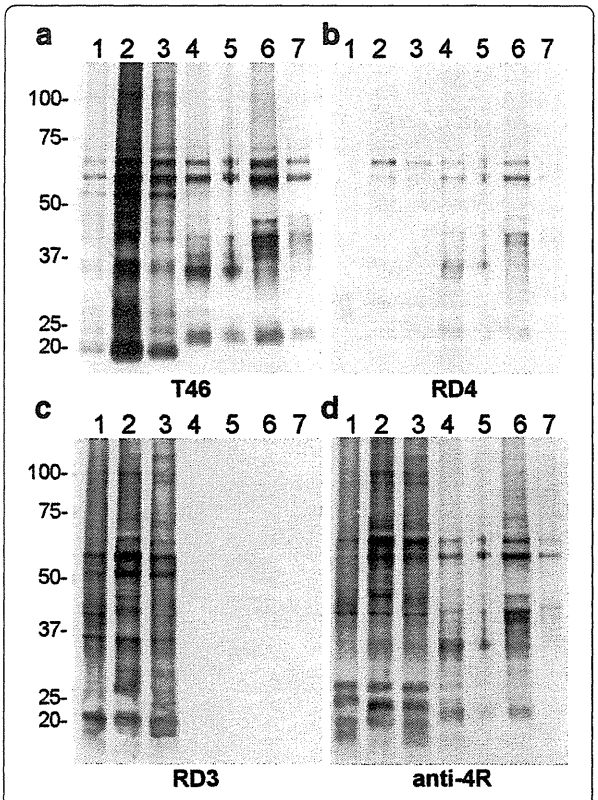

Figure 3 New anti-4R strongly stained tau bands and smears in AD. Immunoblot analyses of Sarkosyl-insoluble tau from three AD (1–3), two PSP(4, 5) and two CBD (6, 7) cases with T46 (**a**, 1:2000 dilution), RD4 (**b**, 1:1000 dilution), RD3 (**c**, 1:1000 dilution) and anti-4R antibodies (**d**, 1:2000 dilution).

especially in RD3+/RD4– NFTs. RD3 stained abundant ghost tangles in entorhinal cortex and NFTs in CA1, but failed to stain fine processes of NFTs and NTs (Figure 4), as previously reported [10]. Anti-4R also failed to detect ghost tangles in entorhinal cortex.

Deamidation of N279 reduces the ability of tau to bind microtubules

N279 is located in one of the repeat regions of tau that are involved in binding to microtubules. Therefore, we tested whether the deamidation influences the role of tau in microtubule binding and assembly. First, the ability of N279D mutant tau to mediate polymerization of tubulin was compared to that of wild-type tau by monitoring the turbidity after mixing tubulin with tau. The N279D mutant tau showed a reduced ability to promote microtubule assembly (Figure 5a). We next investigated the binding ability of the N279D mutant tau to taxol-stabilized microtubules. Tau bound and unbound to microtubules was separated by centrifugation and the levels were quantitated by means of SDS-PAGE and CBB staining (Figure 5b,c). When the amount of tau was

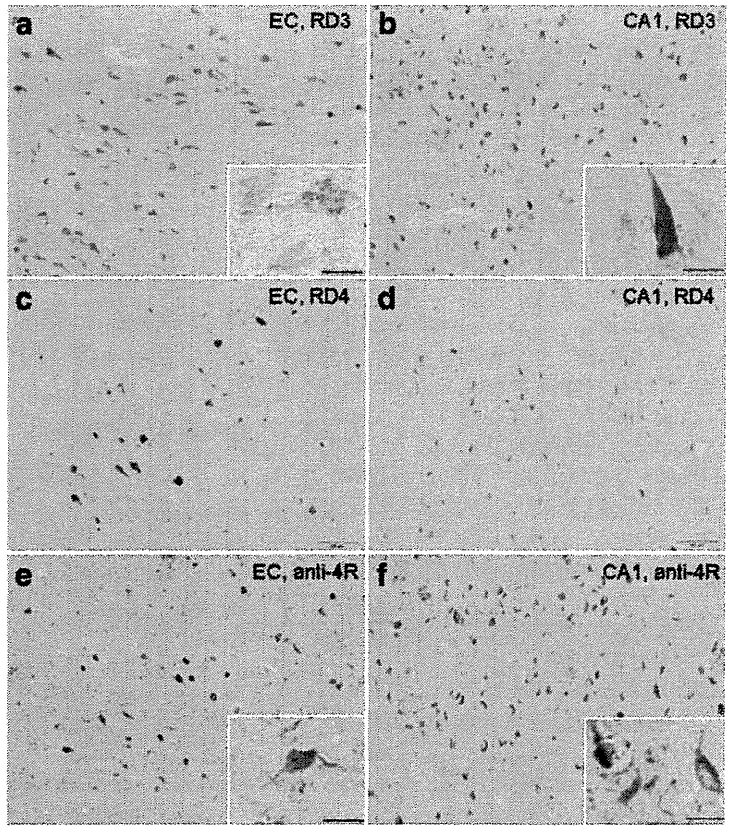

Figure 4 New anti-4R antibody stained intracellular NFTs more extensively than did RD4. Immunostaining of entorhinal cortex (EC) and CA1 sections of AD brain after autoclaving and formic acid treatments, using RD3 **(a, b)**, RD4 **(c, d)** and anti-4R **(e, f)** antibodies. NFTs with higher magnification are shown in insets. Bar = 100 μm (25 μm in insets).

increased in the presence of a constant amount of microtubules, the binding affinity and the microtubule assembly-promoting activity of N279D mutant tau were both found to be much lower than those of WT tau, clearly indicating that deamidation of N279 reduced the functional activity of tau (Figure 5b,c). Since several positively charged residues have been shown to be important for the ability of tau to promote microtubule assembly, negative charge arising from deamidation of N279 may affect the interaction.

Discussion

Our present results indicate that the N279 on the RD4 epitope is extensively deamidated in pathological tau from AD brain. Because the widely used RD4 antibody is unreactive to the deamidated epitope, the level of 4R tau isoforms in AD brain will have been markedly underestimated in previous immunohistochemical and biochemical analyses using RD4 antibody. Deamidation is an irreversible, non-enzymatic reaction, in which the amide-containing side chain is removed from asparagine or glutamine. It is known to be a marker for aging in proteins with long life-spans, and, for example, many deamidation sites have been identified in crystallins [11], the major proteins of the eye lens. In biochemical deamidation, the side chain of an asparagine residue attacks the amide group, forming a succinimide intermediate, which, upon hydrolysis, affords either aspartate or isoaspartate [12]. Isoaspartate formation from asparagine residues of tau has been reported in AD brains [9,13], but deamidation has been less well investigated. Nevertheless, deamidation is important because it alters the charge of the amino acid residue, and this can markedly affect protein structure and interaction with other proteins. Therefore, deamidation of N279 may have an effect on tau similar to that of missense mutations in FTDP-tau, many of which affect the ability of tau to promote microtubule assembly or to self-aggregate into amyloid fibrils. Indeed, substitution of N279 to Asp greatly reduced the ability of tau to promote microtubule assembly (Figure 5). However, we did not observe any accelerating effect on tau fibril formation (data not shown). Further studies are needed, but it is possible that the deamidation may be a consequence of aging of tau in paired helical filaments (PHF).

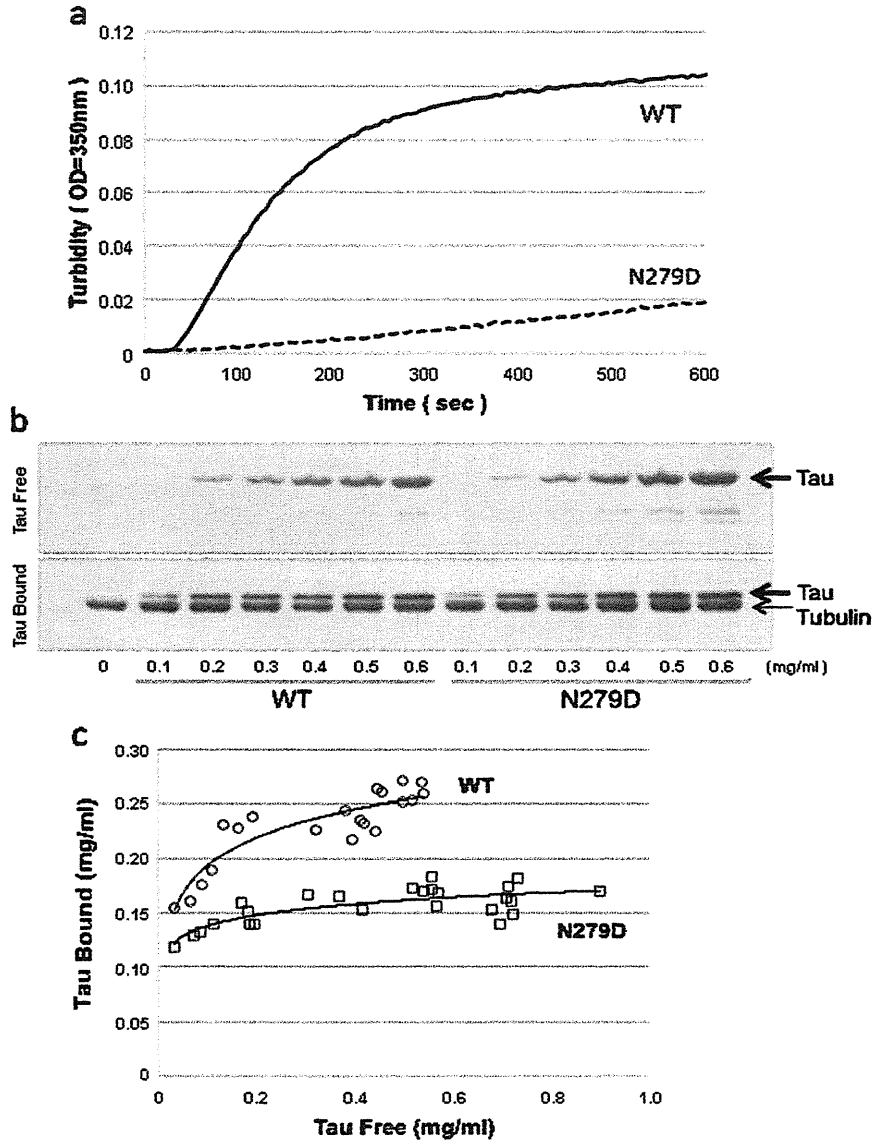

Figure 5 Deamidation of N279 reduced the functional activity of tau. Effects of deamidation at N279 on the ability of four repeat htau46 (412 amino acid isoform of human tau) to promote microtubule assembly **(a)** and to bind to microtubules **(b, c)**. **a**, Polymerisation of tubulin induced by wild-type htau46 (solid line) and htau46 N279D (dotted line) was monitored by turbidimetry. Results of a typical experiment are shown; similar results were obtained in three separate experiments. **b**, SDS-PAGE and CBB stainings of free tau and tau bound (arrows) to a constant amount of tubulin (small arrow) are shown. **c**, Scatter plots of quantitations of free tau and tau bound to WT tau (open circles) and N279D mutant tau (open squares).

Other potential post-translational modifications in the RD4 epitope include acetylation and methylation on K280 [14-16]. Using antibodies specific for tau acetylated at lysine 280, significant acetylated-tau pathology has been found with a distribution pattern similar to that of hyperphosphorylated tau [15]. However, in our protein chemical analyses (including LC/MS/MS) of AD tau, such modification has not been clearly detected. It is possible that the modification is hardly detectable in LC/MS/MS. But it is also possible that antibodies to acetylated K280 peptide may recognize a tau epitope exposed as a result of conformational change. It remains to be investigated whether the acetylation or methylation alters immunoreactivity to RD4 or whether deamidation of N279 influences immunoreactivity to acetylated K280.

The results of this study have implications for the molecular mechanisms of tau assembly. The RD4 immunoreactivity of AD tau (composed of 3R and 4R tau) is

different from that of CBD tau and PSP tau (composed of 4R tau), suggesting that the tau filament core structures may be different. Indeed, abnormal tau filaments characteristic of each disease have been described [17]. It seems reasonable to speculate that the RD4 epitope is integrated in the filament cores in CBD and PSP, making it resistant to deamidation and degradation. However, further analyses will be needed to understand the structures of tau in CBD, PSP and other tauopathies.

Prion-like spreading of intracellular pathological proteins or template (seed)-dependent conversion of normal protein to abnormal forms are candidate molecular mechanisms for involvement in the pathogenesis and progression of neurodegenerative diseases including AD [18-21]. The biochemical and structural differences of tau in AD from that in 4R tauopathies found in this study may therefore have implications for prion-like propagation of tau. Heterodimeric tau composed of both 3R tau and 4R tau with an amyloid-like conformation may act as a template for converting normal 3R and 4R tau to the abnormal structures seen in neurons, forming unique PHF structures composed of both 3R and 4R tau. Therefore, site-specific antibodies are important tools for immunohistochemical and biochemical studies of the role of tau in neurodegenerative diseases.

Conclusions

We conclude that extensive irreversible post-translational deamidation takes place at asparagine residue 279 (N279) in the RD4 epitope of tau in Alzheimer's disease (AD), but not corticobasal degeneration (CBD) or progressive supranuclear palsy (PSP), and this modification abrogates the immunoreactivity to RD4. An antiserum raised against deamidated RD4 peptide specifically recognized 4R tau isoforms, regardless of deamidation, and strongly stained tau in AD brain.

Methods

Human brain tissues

Human brain tissues were obtained from The Manchester Brain Bank, University of Manchester (Manchester, UK), Tokyo Metropolitan Institute of Gerontology (Tokyo, Japan) and NCNP Hospital (Tokyo, Japan). This study was approved by the local research ethics committees of Tokyo Institute of Psychiatry and Tokyo Metropolitan Institute of Medical Science. The subjects included three patients diagnosed with AD, three with PSP and three with CBD, neuropathologically confirmed by immunohistochemistry with antibodies to tau, Aβ, α-synuclein and TDP-43.

Preparation of sarkosyl-insoluble fractions

Brain samples (0.5 g) from patients with AD, PSP and CBD were each homogenized in 10 ml of homogenization buffer (HB: 10 mM Tris–HCl, pH 7.5 containing 0.8 M NaCl, 1 mM EGTA, 1 mM dithiothreitol). Sarkosyl was added to the lysates (final concentration: 2%), which were then incubated for 30 min at 37°C and centrifuged at 20,000 g for 10 min at 25°C. The supernatant was divided into eight tubes (each 1.3 mL) and centrifuged at 100,000 g for 20 min at 25°C. The pellets were further washed with sterile saline (0.5 mL/tube) and centrifuged at 100,000 g for 20 min. The resulting pellets were used as Sarkosyl-insoluble fraction (ppt).

LC/MS/MS analysis of sarkosyl-insoluble tau

Sarkosyl-insoluble tau from AD brains was subjected to SDS–PAGE using 4–20% polyacrylamide gel (PAGE mini, Daiichi, Tokyo). After staining with Coomassie brilliant blue R-250 (CBB), the bands corresponding to the phosphorylated tau (64 and 68 kDa) were cut out. In-gel digestion of proteins with 1 μg/ml trypsin was carried out as described previously and the resulting peptides were analyzed by an ion-trap spectrometry (Velos Pro; Thermo Fisher Scientific Inc. Waltham, MA). The MS/MS data files were searched and analyzed using the Mascot Server (Matrix Science Inc., Boston, MA).

Recombinant tau proteins

Expression constructs for six human tau isoforms in plasmid pRK172 were kindly provided by Dr. Goedert. Site-directed mutagenesis was used to change N279 to Asp (numbering refers to the 441-amino-acid isoform of human brain tau) in the four-repeat 412-amino-acid isoform (expressed from cDNA clone htau46). Wild-type and mutated tau proteins were expressed in *Escherichia coli* BL21(DE3) and purified as described previously[22]. For *in vitro* phosphorylation, purified tau (10 μg/ml) was incubated with PKA (10,000 U/ml; New England Biolabs, Beverly, MA) in 30 mM Tris–HCl buffer (pH 7.5) containing 0.1 mM EGTA, 10 mM $MgSO_4$, 0.8 mM PMSF and 2 mM ATP, at 30°C for 1 hr.

Antibodies

RD3 (directed to residues 209~224: Millipore), RD4 (residues 275~291: Millipore), T46 (residues 404~441: Invitrogen) and pS396 (phospho-Ser396: Calbiochem) were purchased. Antiserum anti-4R was raised against a synthetic peptide VQIIDKKLDLSNVQSKC which corresponds to residues 275~291 of human tau (441 residues), with substitution of N279 to Asp (Sigma Aldrich Japan). The peptide was conjugated to m-maleimidobenzoyl- N-hydrosuccinimide ester-activated keyhole limpet hemocyanin (KLH). The KLH-peptide complex (1 mg of each immunogen) emulsified in Freund's complete adjuvant was injected subcutaneously into a New Zealand White rabbit, followed by 5 weekly subcutaneous injections of 150 μg KLH-peptide complex emulsified in Freund's

incomplete adjuvant, starting 3 weeks after the first immunization.

ELISA assay

Each synthetic peptide consisting of residues 275~291 (VQIINKKLDLSNVQSKC) with the fifth position being replaced by L-Asp, L-isoAsp, or D-Asp was synthesized by the solid-phase method (Sigma Aldrich Japan) These peptides, L-Asn (wild-type), L-Asp, L-isoAsp, D-Asp (0.625 ~ 10 μg/ml in 50 mM Tris–HCl, pH 8.8) were coated onto microtitre plates (SUMILON) at 4°C for 16 h. The plates were blocked with 10% fetal bovine serum (FBS) in PBS, incubated with the first antibodies (RD4, 1:1000; anti-4R, 1:3000) diluted in 10% FBS/PBS at room temperature for 1.5 h, followed by incubation with HRP-goat anti-rabbit IgG (Bio-Rad) at 1:1000 dilution, and reacted with the substrate, 0.4 mg/ml o-phenylendiamine, in citrate buffer (24 mM citric acid, .51 mM Na_2HPO_4), The absorbance at 490 nm was measured using Plate Chameleon (HIDEX) as described [23].

Microtubule assembly and tau binding

Purified recombinant wild-type and mutant tau (htau46) proteins (0.1 mg/ml, 2.3 μM) were incubated with bovine brain tubulin (1 mg/ml, 20 μM, cytoskeleton) in assembly buffer at 37°C, as described [22]. The assembly of tubulin was monitored in terms of the change in turbidity at 350 nm. The binding assay was performed as described [24]. Briefly, purified tubulin was incubated at 37°C in the presence of 1 mM GTP and 20 μM taxol. Tau protein was added at various concentrations and each mixture was incubated for 10 min. The suspensions were centrifuged for 100,000 g at 37°C. The resulting pellets were resuspended in 50 mM PIPES pH 6.9, 1 mM EGTA, 0.2 mM $MgCl_2$, 5 mM DTT, 0.5 M NaCl. The pellets and supernatants (containing bound and free tau, respectively) were subjected to SDS-PAGE and stained with Coomassie brilliant blue R250. The gels were scanned at 400 dpi on a gel scanner and evaluated using the software provided.

Gel electrophoresis and immunoblotting

Samples were run on gradient 4-20% or 10% polyacrylamide gels and electrophoretically transferred to PVDF membranes. Residual protein-binding sites were blocked by incubation with 3% gelatin (Wako) for 10 min at 37°C, followed by overnight incubation at room temperature with the primary antibody. The membrane was then incubated for 1 hr at room temperature with anti-rabbit IgG (BA-1000, Vector Lab) or anti-mouse IgG (BA-2000, Vector lab), then incubated for 30 min with avidin-horseradish peroxidase (Vector Lab), and the reaction product was visualized by using 0.1% 3,3-diaminobenzidine (DAB) and 0.2 mg/ml $NiCl_2$ as the chromogen.

Immunohistochemistry

Formalin-fixed paraffin-embedded sections of AD brains were used for immunohistochemistry. The sections were pretreated by autoclaving for 10 min in 10 mM sodium citrate buffer at 120°C and treated with 100% formic acid for 10 min. Sections were washed with 10 mM phosphate-buffered saline (PBS, pH 7.4) three times for 10 min each. Sections were blocked with 10% normal serum and incubated overnight at room temperature with one of the primary antibodies in PBS. After washing, sections were incubated with biotinylated anti-mouse or rabbit secondary antibody for 2 h, followed by biotinylated horseradish peroxidase complex (ABC, Vector) for 1 hr. The label was visualized with EnVision™(Dako). Sections were counterstained with hematoxylin.

Competing interests

The authors declare that they have no competing interests.

Authors' contributions

AD, MT, MS and TN performed biochemical and immunochemical studies. FK performed LC/MS/MS analysis. HK performed immunohistochemistry. TA helped for characterisation of antibody. HA, YS, HH, SM and DM performed neuropathological studies and analyses. MH performed study design, preparation of antibody, biochemical analyses and wrote the paper. All authors read and approved the final manuscript.

Acknowledgements

We acknowledge the support of Alzheimer's Research UK and Alzheimer's Society through their funding of the Manchester Brain Bank under the Brains for Dementia Research (BDR) initiative. This work was supported by a Grant-in-Aid for Scientific Research (S) (JSPS KAKENHI 23228004 to M.H.), a Grant-in-Aid for Scientific Research (A) (JSPS KAKENHI 23240050 to M.H.), MHLW Grant (Number 12946221 to M.H.) and a Grant-in-Aid for Scientific Research on Innovative Area 'Brain Environment' (MEXT KAKENHI 24111556 to T.N).

Author details

[1]Department of Neuropathology and Cell Biology, Tokyo Metropolitan Institute of Medical Science, Setagaya-ku, Tokyo 156-8506, Japan. [2]Histology center, Tokyo Metropolitan Institute of Medical Science, Setagaya-ku, Tokyo 156-8506, Japan. [3]Dementia Research Project, Tokyo Metropolitan Institute of Medical Science, Setagaya-ku, Tokyo 156-8506, Japan. [4]Department of Applied Biological Science, Faculty of Science and Technology, Tokyo University of Science, 2641 Yamazaki, Noda-shi, Chiba-ken 278-8510, Japan. [5]Centre for Clinical and Cognitive Neuroscience, Institute of Brain Behavior and Mental Health, University of Manchester, Salford M6 8HD, UK. [6]Department of Laboratory Medicine, National Center Hospital, NCNP, 4-1-1 Ogawahigashi, Kodaira, Tokyo 187-8502, Japan. [7]Department of Neuropathology, Tokyo Metropolitan Institute of Gerontology, Itabashi-ku, Tokyo 173-0015, Japan.

Received: 17 August 2013 Accepted: 17 August 2013
Published: 21 August 2013

References

1. Umeda Y, Taniguchi S, Arima K, Piao YS, Takahashi H, Iwatsubo T, Mann D, Hasegawa M: **Alterations in human tau transcripts correlate with those of neurofilament in sporadic tauopathies.** *Neurosci Lett* 2004, **359**:151–154.
2. Goedert M, Spillantini MG: **Pathogenesis of the tauopathies.** *J Mol Neurosci* 2011, **45**:425–431.
3. Arai T, Ikeda K, Akiyama H, Nonaka T, Hasegawa M, Ishiguro K, Iritani S, Tsuchiya K, Iseki E, Yagishita S, Oda T, Mochizuki A: **Identification of amino-terminally**

cleaved tau fragments that distinguish progressive supranuclear palsy from corticobasal degeneration. *Ann Neurol* 2004, **55**:72–79.
4. de Silva R, Lashley T, Gibb G, Hanger D, Hope A, Reid A, Bandopadhyay R, Utton M, Strand C, Jowett T, Khan N, Anderton B, Wood N, Holton J, Revesz T, Lees A: **Pathological inclusion bodies in tauopathies contain distinct complements of tau with three or four microtubule-binding repeat domains as demonstrated by new specific monoclonal antibodies.** *Neuropathol Appl Neurobiol* 2003, **29**:288–302.
5. de Silva R, Lashley T, Strand C, Shiarli AM, Shi J, Tian J, Bailey KL, Davies P, Bigio EH, Arima K, Iseki E, Murayama S, Kretzschmar H, Neumann M, Lippa C, Halliday G, MacKenzie J, Ravid R, Dickson D, Wszolek Z, Iwatsubo T, Pickering-Brown SM, Holton J, Lees A, Revesz T, Mann DM: **An immunohistochemical study of cases of sporadic and inherited frontotemporal lobar degeneration using 3R- and 4R-specific tau monoclonal antibodies.** *Acta Neuropathol* 2006, **111**:329–340.
6. Togo T, Akiyama H, Iseki E, Uchikado H, Kondo H, Ikeda K, Tsuchiya K, de Silva R, Lees A, Kosaka K: **Immunohistochemical study of tau accumulation in early stages of Alzheimer-type neurofibrillary lesions.** *Acta Neuropathol* 2004, **107**:504–508.
7. Piao YS, Tan CF, Iwanaga K, Kakita A, Takano H, Nishizawa M, Lashley T, Revesz T, Lees A, de Silva R, Tsujihata M, Takahashi H: **Sporadic four-repeat tauopathy with frontotemporal degeneration, parkinsonism and motor neuron disease.** *Acta Neuropathol* 2005, **110**:600–609.
8. Hasegawa M, Morishima-Kawashima M, Takio K, Suzuki M, Titani K, Ihara Y: **Protein sequence and mass spectrometric analyses of tau in the Alzheimer's disease brain.** *J Biol Chem* 1992, **267**:17047–17054.
9. Watanabe A, Takio K, Ihara Y: **Deamidation and isoaspartate formation in smeared tau in paired helical filaments. Unusual properties of the microtubule-binding domain of tau.** *J Biol Chem* 1999, **274**:7368–7378.
10. Hara M, Hirokawa K, Kamei S, Uchihara T: **Isoform transition from four-repeat to three-repeat tau underlies dendrosomatic and regional progression of neurofibrillary pathology.** *Acta Neuropathol* 2013, **125**:565–579.
11. Van Kleef FS, De Jong WW, Hoenders HJ: **Stepwise degradations and deamidation of the eye lens protein alpha-crystallin in ageing.** *Nature* 1975, **258**:264–266.
12. Geiger T, Clarke S: **Deamidation, isomerization, and racemization at asparaginyl and aspartyl residues in peptides. Succinimide-linked reactions that contribute to protein degradation.** *J Biol Chem* 1987, **262**:785–794.
13. Miyasaka T, Watanabe A, Saito Y, Murayama S, Mann DM, Yamazaki M, Ravid R, Morishima-Kawashima M, Nagashima K, Ihara Y: **Visualization of newly deposited tau in neurofibrillary tangles and neuropil threads.** *J Neuropathol Exp Neurol* 2005, **64**:665–674.
14. Cohen TJ, Guo JL, Hurtado DE, Kwong LK, Mills IP, Trojanowski JQ, Lee VM: **The acetylation of tau inhibits its function and promotes pathological tau aggregation.** *Nat Commun* 2011, **2**:252.
15. Irwin DJ, Cohen TJ, Grossman M, Arnold SE, Xie SX, Lee VM, Trojanowski JQ: **Acetylated tau, a novel pathological signature in Alzheimer's disease and other tauopathies.** *Brain* 2012, **135**:807–818.
16. Min SW, Cho SH, Zhou Y, Schroeder S, Haroutunian V, Seeley WW, Huang EJ, Shen Y, Masliah E, Mukherjee C, Meyers D, Cole PA, Ott M, Gan L: **Acetylation of tau inhibits its degradation and contributes to tauopathy.** *Neuron* 2010, **67**:953–966.
17. Arima K: **Ultrastructural characteristics of tau filaments in tauopathies: immuno-electron microscopic demonstration of tau filaments in tauopathies.** *Neuropathology* 2006, **26**:475–483.
18. Clavaguera F, Akatsu H, Fraser G, Crowther RA, Frank S, Hench J, Probst A, Winkler DT, Reichwald J, Staufenbiel M, Ghetti B, Goedert M, Tolnay M: **Brain homogenates from human tauopathies induce tau inclusions in mouse brain.** *Proc Natl Acad Sci U S A* 2013, **110**:9535–9540.
19. Masuda-Suzukake M, Nonaka T, Hosokawa M, Oikawa T, Arai T, Akiyama H, Mann DM, Hasegawa M: **Prion-like spreading of pathological alpha-synuclein in brain.** *Brain* 2013, **136**:1128–1138.
20. Hasegawa M, Nonaka T, Tsuji H, Tamaoka A, Yamashita M, Kametani F, Yoshida M, Arai T, Akiyama H: **Molecular dissection of TDP-43 proteinopathies.** *J Mol Neurosci* 2011, **45**:480–485.
21. Nonaka T, Masuda-Suzukake M, Arai T, Hasegawa Y, Akatsu H, Obi T, Yoshida M, Murayama S, Mann DM, Akiyama H, Hasegawa M: **Prion-like Properties of Pathological TDP-43 Aggregates from Diseased Brains.** *Cell Rep* 2013, **4**:124–134.
22. Hasegawa M, Smith MJ, Goedert M: **Tau proteins with FTDP-17 mutations have a reduced ability to promote microtubule assembly.** *FEBS Lett* 1998, **437**:207–210.
23. Masuda M, Hasegawa M, Nonaka T, Oikawa T, Yonetani M, Yamaguchi Y, Kato K, Hisanaga S, Goedert M: **Inhibition of alpha-synuclein fibril assembly by small molecules: analysis using epitope-specific antibodies.** *FEBS Lett* 2009, **583**:787–791.
24. Gustke N, Steiner B, Mandelkow EM, Biernat J, Meyer HE, Goedert M, Mandelkow E: **The Alzheimer-like phosphorylation of tau protein reduces microtubule binding and involves Ser-Pro and Thr-Pro motifs.** *FEBS Lett* 1992, **307**:199–205.

doi:10.1186/2051-5960-1-54
Cite this article as: Dan *et al.*: **Extensive deamidation at asparagine residue 279 accounts for weak immunoreactivity of tau with RD4 antibody in Alzheimer's disease brain.** *Acta Neuropathologica Communications* 2013 **1**:54.

Acta Neuropathol
DOI 10.1007/s00401-013-1191-9

CORRESPONDENCE

3R and 4R tau isoforms in paired helical filaments in Alzheimer's disease

Masato Hasegawa · Sayuri Watanabe · Hiromi Kondo · Haruhiko Akiyama · David M. A. Mann · Yuko Saito · Shigeo Murayama

Received: 20 August 2013 / Revised: 29 September 2013 / Accepted: 30 September 2013

Isoform-specific tau antibodies RD3 and RD4 are useful tools for investigating expression and localization of three-repeat (3R) and four-repeat (4R) tau isoforms. Recently, transition from 3R to 4R tau in Alzheimer's disease (AD) was proposed based on immunohistochemical studies with RD3 and RD4 [3]. Here, we show that two factors influence immunoreactivity to these antibodies. First, deamidation at the RD4 epitope abrogates immunoreactivity to RD4, and second, presentation of RD3 and RD4 epitopes is reciprocally affected by protease. Asparagine at position 279 in the RD4 epitope is predominantly deamidated to aspartic acid in pathological tau in AD brains [2, 4]. Consequently, the presence of 4R tau in AD pathologies may be underestimated when RD4 is used. However, anti-4R (available from Cosmo Bio Co., Ltd.) raised against RD4 peptide with N279D substitution stained both wild-type and deamidated 4R tau, and strongly stained RD3+/RD4− tangles and smearing tau fragments in Sarkosyl-insoluble fraction of AD brain [2].

It was reported that RD3 stained abundant ghost tangles in entorhinal cortex and tangles in CA1, but failed to stain fine processes of tangles and threads [3], while RD4 failed to detect ghost tangles in entorhinal cortex [3]. To understand these findings, we examined the influence of protease on immunoreactivity. Paraffin sections of AD brains were treated with 10 μg/mL Proteinase K (Pro-K) for 30 min after autoclaving (Ac) and formic acid (FA) treatment. RD3 staining was strongly enhanced (Fig. 1a, b). Conversely, RD4 immunoreactivity almost completely disappeared after Pro-K treatment (Fig. 1c, d). Not only ghost tangles but also RD3−/RD4+ tangles and their processes became RD3-positive after Pro-K treatment (Fig. 1a, b), strongly suggesting that the RD3 epitope was buried in tau filaments of intracellular tangles and threads, and was exposed by Pro-K treatment. Contrary to expectation, anti-4R staining was also enhanced by Pro-K treatment (Fig. 1e, f). It is possible that the recognition site of anti-4R is distinct from that of RD4 and is exposed by Pro-K treatment of sections. Anti-4R antibody may recognize the carboxyl-half of the antigen peptide, while RD4 recognizes the amino-terminal half around N279. Pro-K treatment was also effective in immunostaining of free-floating AD sections with a lower concentration.

To confirm these findings biochemically, Sarkosyl-insoluble fractions from two AD brains were treated with trypsin or Pro-K, then immunoblotted with RD3, RD4, anti-4R and anti-pS396 (Fig. 1g–j). RD3 strongly stained many bands and smears, as seen with pS396 (Fig. 1g, j),

M. Hasegawa (✉) · S. Watanabe
Department of Neuropathology and Cell Biology, Tokyo Metropolitan Institute of Medical Science, Setagaya-ku, Tokyo 156-8506, Japan
e-mail: hasegawa-ms@igakuken.or.jp

H. Kondo
Histology Center, Tokyo Metropolitan Institute of Medical Science, Setagaya-ku, Tokyo 156-8506, Japan

H. Akiyama
Dementia Research Project, Tokyo Metropolitan Institute of Medical Science, Setagaya-ku, Tokyo 156-8506, Japan

D. M. A. Mann
Centre for Clinical and Cognitive Neuroscience, Institute of Brain Behavior and Mental Health, University of Manchester, Salford M6 8HD, UK

Y. Saito
Department of Laboratory Medicine, National Center Hospital, NCNP, 4-1-1 Ogawahigashi, Kodaira, Tokyo 187-8502, Japan

S. Murayama
Department of Neuropathology, Tokyo Metropolitan Institute of Gerontology, Itabashi-ku, Tokyo 173-0015, Japan

Published online: 09 November 2013

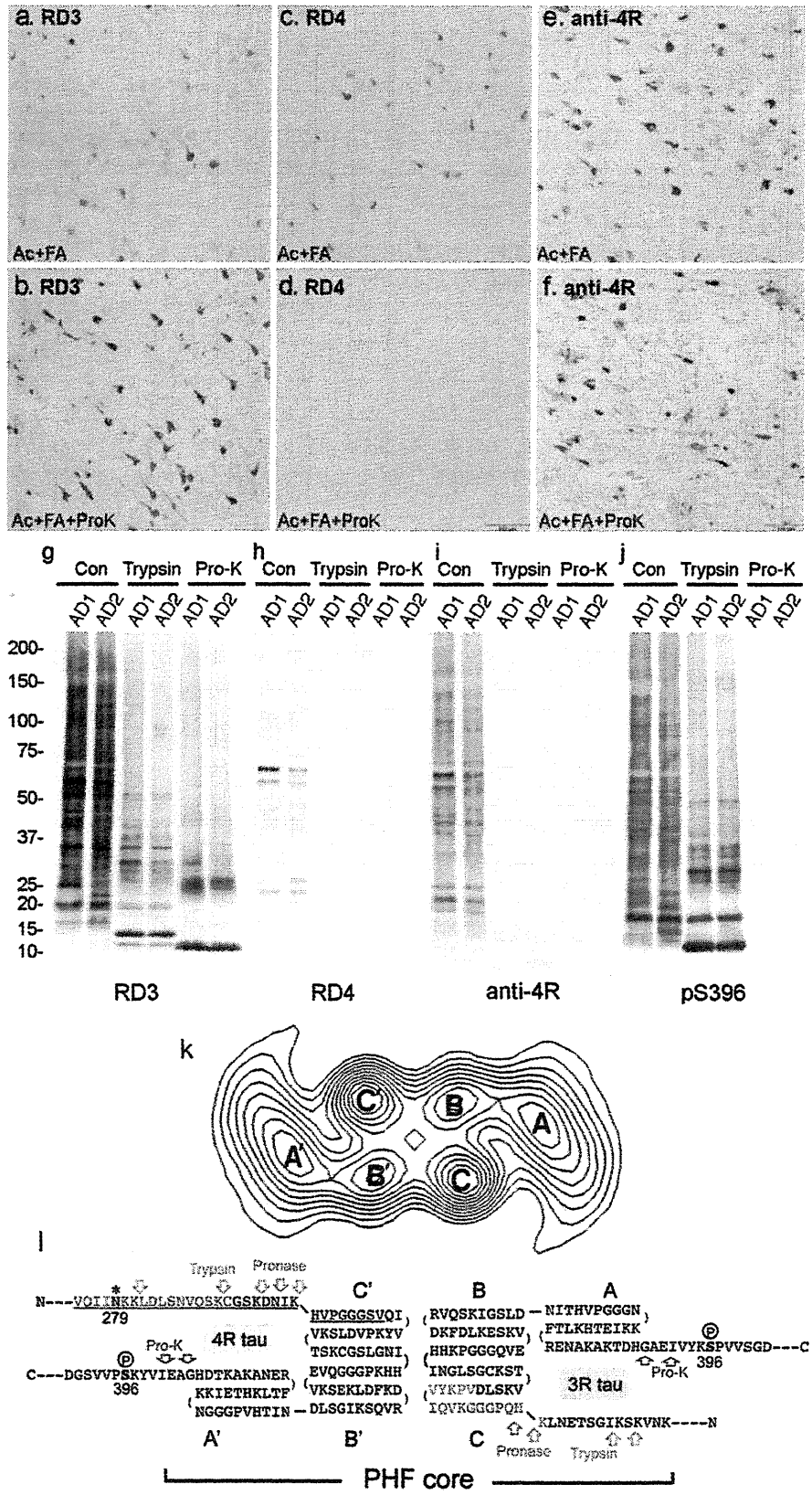

Fig. 1 **a–f** Immunostaining of AD sections after Ac and FA treatment before (**a**, **c**, **e**) and after (**b**, **d**, **f**) Pro-K treatment, using RD3 (**a**, **b**), RD4 (**c**, **d**) and anti-4R (**e**, **f**). *Bar* 100 μm. **g–j** Immunoblots of Sarkosyl-insoluble tau from two AD brains, before (*Con*) and after treatments with trypsin or Pro-K, using RD3 (**g**), RD4 (**h**), anti-4R (**i**) and pS396 (**j**). **k–l** Computed cross-section through a paired helical filament (**k**) [reproduced from Ref. [1], with permission of the publisher], a predicted folding model of 3R and 4R tau in PHF (**l**). RD3 and RD4 epitopes are indicated by *blue* and *red*, respectively. 4R tau specific insertion is indicated by *underlining*. The deamidation site N279 is indicated by *asterisks*. Phosphorylation of Ser396 is indicated. Possible trypsin, pronase and Pro-K cleavage sites are indicated in *green*, *purple* and *dark blue arrows*, respectively. The protease-resistant domain of PHF is indicated as *PHF-core*

whereas RD4 only labeled the 64/68 kDa doublet and some fragments at ~25 kDa (Fig. 1h). Anti-4R strongly stained the smears and fragments (Fig. 1i), suggesting that tau in these RD4-negative anti-4R-positive bands and smears is deamidated at N279. The weak RD4 and strong anti-4R immunoreactivities were completely abolished after trypsin or Pro-K treatment (Fig. 1h, i). This result is inconsistent with the immunohistochemistry, but protease sensitivity is likely different in fixed tissues. In contrast, the RD3 epitope was retained in the fragments, and RD3 strongly reacted with the protease-resistant 10–25 kDa bands after trypsin or Pro-K treatment (Fig. 1g). pS396 epitope was removed by Pro-K but not trypsin, suggesting a location outside the PHF core. Trypsin may not cleave the KSP site because of phosphorylation of Ser396. These results demonstrate reciprocal effects of protease treatment on RD3 and RD4 epitopes, indicating that RD4 epitope in tau in AD is susceptible to proteases, while RD3 epitope is highly resistant.

These results are consistent with previous findings. Wischik et al. identified two types of amino acid sequences, QPGGGKVQIVYK... (3R tau) and IKXVPGG... (4R tau), in 12-kDa tau fragment comprising the pronase-resistant core of PHFs [6] (see Fig. 1k). We identified HQPGGG... (3R tau) and HVPGGG... (4R tau) in 7–15 kDa trypsin-resistant fragments of PHF-tau in AD brains [5]. In both cases, 3R and 4R tau isoforms were detected, but the 4R tau N-terminus lacked the RD4 epitope. Based on these observations and a computed cross-section of PHF (Fig. 1k) [1], we propose a schematic model of tau folding in PHF (Fig. 1l). Analysis of the cross-sectional density in the PHF core on electron micrographs indicates the presence of two C-shaped morphological units, which correspond to the two strands of PHF, each with three domains (Fig. 1k) [1]. The RD3 epitope is buried in the PHF core and is normally masked by the N- or C-terminal region of tau, but is exposed in ghost tangles and/or in PHFs attacked by proteases. The RD4 epitope, which is mostly deamidated in PHF, is located slightly outside the core, where it can be digested by proteases (Fig. 1l). This model can explain the epitope masking of RD3 and RD4 and the reciprocal effects of degradation or protease treatment on the immunoreactivities.

This study indicates that differential presentation of epitopes can occur as a result of folding and processing, even when the epitopes are located in close proximity. Tau in PHFs appears to be processed gradually by intracellular proteases and more extensively in extracellular space during AD progression. We suggest that changes in immunoreactivity to antibodies reflect aging of tau in tangles or PHFs, which are composed of both 3R and 4R tau isoforms. We also show that Pro-K treatment of sections after Ac and FA treatment is useful for unmasking buried epitopes.

Acknowledgments We acknowledge the support of Alzheimer's Research UK and Alzheimer's Society through their funding of Manchester Brain Bank under the Brains for Dementia Research (BDR) initiative. This work was supported by Grants-in-Aid for Scientific Research (S) (JSPS KAKENHI 23228004), (A) (JSPS KAKENHI 23240050), and MHLW Grant 12946221 (to M.H.).

References

1. Crowther RA (1991) Straight and paired helical filaments in Alzheimer disease have a common structural unit. Proc Natl Acad Sci USA 88:2288–2292
2. Dan A, Takahashi M, Masuda-Suzukake M, Kametani F, Nonaka T, Kondo H, Akiyama H, Arai T, Mann DM, Saito Y, Hatsuta H, Murayama S, Hasegawa M (2013) Extensive deamidation at asparagine residue 279 accounts for weak immunoreactivity of tau with RD4 antibody in Alzheimer's disease brain. Acta Neuropathol Commun 1:54
3. Hara M, Hirokawa K, Kamei S, Uchihara T (2013) Isoform transition from four-repeat to three-repeat tau underlies dendrosomatic and regional progression of neurofibrillary pathology. Acta Neuropathol 125:565–579
4. Hasegawa M, Morishima-Kawashima M, Takio K, Suzuki M, Titani K, Ihara Y (1992) Protein sequence and mass spectrometric analyses of tau in the Alzheimer's disease brain. J Biol Chem 267:17047–17054
5. Hasegawa M, Watanabe A, Takio K, Suzuki M, Arai T, Titani K, Ihara Y (1993) Characterization of two distinct monoclonal antibodies to paired helical filaments: further evidence for fetal-type phosphorylation of the tau in paired helical filaments. J Neurochem 60:2068–2077
6. Wischik CM, Novak M, Thogersen HC, Edwards PC, Runswick MJ, Jakes R, Walker JE, Milstein C, Roth M, Klug A (1988) Isolation of a fragment of tau derived from the core of the paired helical filament of Alzheimer disease. Proc Natl Acad Sci USA 85:4506–4510

Brain Advance Access published March 6, 2013
doi:10.1093/brain/awt037 Brain 2013: Page 1 of 11 | 1

BRAIN
A JOURNAL OF NEUROLOGY

Prion-like spreading of pathological α-synuclein in brain

Masami Masuda-Suzukake,[1] Takashi Nonaka,[1] Masato Hosokawa,[2] Takayuki Oikawa,[1] Tetsuaki Arai,[3] Haruhiko Akiyama,[2] David M. A. Mann[4] and Masato Hasegawa[1]

1 Department of Neuropathology and Cell Biology, Tokyo Metropolitan Institute of Medical Science, 2-1-6 Kamikitazawa, Setagaya-ku, Tokyo 156-8506, Japan
2 Dementia Research Project, Tokyo Metropolitan Institute of Medical Science, 2-1-6 Kamikitazawa, Setagaya-ku, Tokyo, 156-8506, Japan
3 Department of Psychiatry, Graduate School of Comprehensive Human Sciences, University of Tsukuba, 1-1-1, Tennodai, Tsukuba, Ibaraki 305-8575, Japan
4 Centre for Clinical and Cognitive Neuroscience, Institute of Brain Behaviour and Mental Health, University of Manchester, Salford M6 8HD, Manchester, UK

Correspondence to: Masato Hasegawa, Ph.D.
Department of Neuropathology and Cell Biology,
Tokyo Metropolitan Institute of Medical Science,
2-1-6 Kamikitazawa, Setagaya-ku,
Tokyo 156-8506,
Japan
E-mail: hasegawa-ms@igakuken.or.jp

α-Synuclein is the major component of filamentous inclusions that constitute the defining characteristic of neurodegenerative α-synucleinopathies. However, the molecular mechanisms underlying α-synuclein accumulation and spread are unclear. Here we show that intracerebral injections of sarkosyl-insoluble α-synuclein from brains of patients with dementia with Lewy bodies induced hyperphosphorylated α-synuclein pathology in wild-type mice. Furthermore, injection of fibrils of recombinant human and mouse α-synuclein efficiently induced similar α-synuclein pathologies in wild-type mice. C57BL/6J mice injected with α-synuclein fibrils developed abundant Lewy body/Lewy neurite-like pathology, whereas mice injected with soluble α-synuclein did not. Immunoblot analysis demonstrated that endogenous mouse α-synuclein started to accumulate 3 months after inoculation, while injected human α-synuclein fibrils disappeared in about a week. These results indicate that α-synuclein fibrils have prion-like properties and inoculation into wild-type brain induces α-synuclein pathology *in vivo*. This is a new mouse model of sporadic α-synucleinopathy and should be useful for elucidating progression mechanisms and evaluating disease-modifying therapy.

Keywords: α-synuclein; Lewy bodies; Parkinson's disease; propagation

Introduction

Filamentous inclusions composed of α-synuclein in nerve cells or glial cells are the defining neuropathological feature of a group of neurodegenerative diseases including Parkinson's disease, dementia with Lewy bodies, and multiple-system atrophy (Goedert, 2001). In these so-called α-synucleinopathies, α-synuclein is deposited in a hyperphosphorylated form with β-sheet-rich, fibrillar structure (Spillantini *et al.*, 1997, 1998; Baba *et al.*, 1998; Wakabayashi *et al.*, 1998; Fujiwara *et al.*, 2002). Missense mutations (A30P, E46K and A53T) in the α-synuclein gene (Polymeropoulos *et al.*, 1997; Kruger *et al.*, 1998; Zarranz *et al.*, 2004) and multiplications of the region (Singleton *et al.*, 2003; Chartier-Harlin *et al.*, 2004; Ibanez *et al.*, 2004,) have been identified in familial forms of Parkinson's disease and dementia with Lewy bodies, indicating that abnormalities of α-synuclein cause

Received November 24, 2012. Revised January 11, 2013. Accepted January 14, 2013.

these diseases. Neuropathologically, α-synuclein lesions are believed to spread progressively throughout the brain and their spread correlates to the staging of clinical symptoms (Muller *et al.*, 2005), as in the case of tau pathology in Alzheimer's disease (Braak and Braak, 1991). Kordower *et al.* (2008) and Li *et al.* (2008) reported that embryonic neurons transplanted into the striatum of an individual with Parkinson's disease developed Lewy body-like pathologies, suggesting that pathological α-synuclein may be transmissible from diseased neurons to healthy neurons. Recent studies have also shown that exogenous α-synuclein fibrils induced Lewy body pathology in cultured neurons (Desplats *et al.*, 2009; Emmanouilidou *et al.*, 2010; Nonaka *et al.*, 2010; Volpicelli-Daley *et al.*, 2011), transgenic mouse brain (Mougenot *et al.*, 2012; Luk *et al.*, 2012*b*) and wild-type mouse brain (Luk *et al.*, 2012*a*). In addition, a growing body of evidence indicates that self-propagating protein aggregates play central roles in many neurodegenerative diseases, including Parkinson's disease and Alzheimer's disease (Clavaguera *et al.*, 2009; Mougenot *et al.*, 2012; Luk *et al.*, 2012*b*; Stohr *et al.*, 2012). In this work, we have tested whether inoculation of insoluble α-synuclein from brains with dementia with Lewy bodies and synthetic mouse and human α-synuclein fibrils can induce α-synuclein pathology in wild-type mice. As a result, we have established a new mouse model of sporadic α-synucleinopathy using wild-type mice.

Materials and methods

Preparation of recombinant α-synuclein monomer and fibrils

Human and mouse α-synuclein were expressed in *E. coli* BL21 (DE3) cells, as described (Masuda *et al.*, 2006*b*). To avoid the production of α-synuclein dimers induced by misexpression of cysteine-containing α-synuclein, the Y136-TAT construct was used (Masuda *et al.*, 2006*a*). α-Synuclein was purified by boiling, Q-Sepharose® ion exchange chromatography and ammonium sulphate precipitation, before dialysis against 30 mM Tris–HCl, pH 7.5. Recombinant proteins were centrifuged at 113 000*g* for 20 min at 4°C to remove insoluble materials and used as α-synuclein monomer. Protein concentrations were determined as described (Yonetani *et al.*, 2009). Purified human and mouse α-synuclein (7 mg/ml) were incubated at 37°C in a shaking incubator (200 rpm) in 30 mM Tris–HCl, pH 7.5, containing 0.1% NaN_3, for 72 h. α-Synuclein fibrils were pelleted by spinning the assembly mixtures at 113 000*g* for 20 min.

Preparation of the insoluble fraction of dementia with Lewy bodies brain

Fresh frozen brain tissue from a patient with dementia with Lewy bodies (phosphorylated α-synuclein pathology is shown in Supplementary Fig. 9) was homogenized in 18 volumes (w/v) of Buffer A (10 mM Tris-HCl, pH 7.4, 0.8 M NaCl, 1 mM EGTA, and 10% sucrose), and sarkosyl was added to the homogenate at a concentration of 2%. The mixture was incubated for 30 min at 37°C, sonicated and spun at 9100*g* for 10 min at 25°C. The supernatant was further centrifuged at 113 000*g* for 20 min at 25°C, and the sarkosyl-insoluble pellet was washed with Buffer A. The pellet was taken up in saline, sonicated and centrifuged at 800*g* for 5 min. The supernatant was used for stereotaxic injection.

Stereotaxic surgery

Four- to six-month-old female C57BL/6J mice (CLEA Japan, Inc.) anaesthetized with 50 mg/kg pentobarbital sodium were injected with 10 μg of recombinant α-synuclein monomer, fibrils or 5 μl of insoluble fraction of dementia with Lewy bodies brain into substantia nigra (anterior-posterior: −3.0 mm; medial-lateral: −1.3 mm; dorsal-ventral: −4.7 mm from the bregma and dura) using a 10-μl Hamilton syringe. Mice were anaesthetized with isoflurane and killed by decapitation. For immunohistochemistry, brains were fixed in 10% formalin neutral buffer solution (Wako), and for biochemical analysis, brains were snap-frozen on dry ice and stored at −80°C. All experimental protocols were approved by the Animal Care and Use Committee of the Tokyo Metropolitan Institute of Medical Science.

Immunohistochemistry

Brains fixed in 10% formalin were cut on a vibratome (Leica) at 50 μm thickness. The free-floating sections were treated with 0.5% H_2O_2 in methanol for 30 min to inactivate peroxidase and blocked with 10% calf serum in PBS. Sections were immunostained with appropriate antibodies. Antibodies used in this study are summarized in Supplementary Table 1. After incubation with the biotinylated-secondary antibody (Vector), labelling was detected using the ABC staining kit (Vector).

Confocal microscopy

For double-label immunofluorescence for phosphorylated α-synuclein and ubiquitin or phosphorylated α-synuclein and p62, brain sections were incubated overnight at 4°C in a cocktail of 1175 and anti-ubiquitin or anti-p62 antibody. The sections were then washed and incubated in a cocktail of Alexa Fluor® 568-conjugated goat anti mouse IgG (Molecular Probes) and Alexa Fluor® 488-conjugated goat anti mouse IgG (Molecular Probes). After further washing, sections were stained with TO-PRO®-3, coverslipped with VECTASHIELD® (Vector) and observed with a laser-scanning confocal fluorescence microscope (LSM5 PASCAL, Carl Zeiss).

Biochemical analysis

Mouse brains were homogenized in 20 volumes (w/v) of Buffer A, then spun at 100 000*g* for 30 min at 4°C, and the supernatant was retained as buffer-soluble fraction. The pellet was homogenized in 20 volumes of Buffer A containing 1% Triton™ X-100 and incubated for 30 min at 37°C. After centrifugation at 100 000*g*, the Triton™-insoluble pellet was further homogenized in Buffer A containing 1% sarkosyl and incubated at 37°C for 30 min. Samples were spun at 100 000*g* for 30 min. The sarkosyl-pellet was sonicated in 30 mM Tris-HCl, pH 7.4, and used for immunoblotting as sarkosyl-insoluble fraction. The samples were subjected to SDS-PAGE on 12.5% polyacrylamide gel and proteins were electrotransferred onto a polyvinylidene difluoride membrane, probed with appropriate antibodies and detected as described (Nonaka *et al.*, 2009).

Behavioural tests

Open field test

Each mouse was placed in the centre of the open field apparatus (25-cm diameter). Activity was measured by SUPERMEX system (Muromachi Kikai) over 90-min period and analysed by CompACT AMS software ver.3 (Muromachi Kikai). Total activity was measured by counting the number of photobeam interruptions over every 5-min period.

Wire hang test

Neuromuscular strength was tested with a wire hang test. The mouse was placed on a wire mesh, waved gently so that the mouse gripped the wire and then inverted. Latency to fall was recorded with a 300-s cut-off time.

Rotarod test

The Rotarod test, using an accelerating Rotarod (Muromachi Kikai), was performed by placing mice on 9-cm diameter rods and measuring the time each animal was able to maintain its balance on the rod. We used 9-cm rods to make the test more sensitive to motor skill learning (Shiotsuki *et al.*, 2010). The speed of the rotarod accelerated from 0 to 40 rpm over a 5-min period.

Y-maze test

Y-maze apparatus (Muromachi Kikai) consisted of three arms (40 cm × 3 cm) made of grey plastic joined in the middle to form a Y shape. Mice were placed into one of the arms of the maze and allowed to explore freely the maze for an 8-min session. The alternation between arms was recorded.

Intranasal administration of abnormal α-synuclein fibrils

Twenty micrograms of recombinant α-synuclein monomer or preformed fibrils, or 10 μl of insoluble fraction of dementia with Lewy bodies brain, was administered intranasally once a week for 1 month to 10-week-old female C57BL/6J mice (soluble mouse α-synuclein, soluble human α-synuclein, mouse α-synuclein fibrils, human α-synuclein fibrils and dementia with Lewy bodies extracts, $n = 5$ per group). At 21 months after the last administration, mice were anaesthetized with pentobarbital sodium and killed by perfusion with phosphate buffer (pH 7.4) and 4% paraformaldehyde in 0.1% phosphate buffer. Brains were cryosectioned and immunostained as described above.

Results

To investigate whether insoluble α-synuclein fibrils can propagate *in vivo*, we injected recombinant human α-synuclein fibrils into the substantia nigra in the right cerebral hemisphere of C57BL/6J mice. α-Synuclein fibrils were prepared using highly purified recombinant α-synuclein (Supplementary Fig. 1A) by incubation with shaking. Formation of the fibrils was confirmed by electron microscopy (Supplementary Fig. 1B) and thioflavin S assay (data not shown). The fibrils were then collected by ultracentrifugation, sonicated and used for injection. Abnormal phosphorylated α-synuclein-positive structures were observed in the brains of mice injected with human α-synuclein fibrils at 15 months after inoculation (Fig. 1). Phosphorylated α-synuclein pathology was distributed throughout the brain including substantia nigra, amygdala, dentate gyrus, hippocampal CA1-3, molecular layer of hippocampus, fimbria, stria terminalis, hypothalamus, somatosensory area, visual cortex, cingulate cortex and corpus callosum (Fig. 1). Phosphorylated α-synuclein-positive structures were also positive for anti-ubiquitin and p62 antibodies (Fig. 2A). Co-localization was confirmed by confocal microscopy (Fig. 2B and C), indicating that these structures have the same immunoreactive properties as Lewy bodies (Kuusisto *et al.*, 2001). By contrast, no phosphorylated α-synuclein, ubiquitin or p62-positive pathology was observed in the brains of mice injected with soluble human α-synuclein (Supplementary Fig. 2). Remarkably, despite the unilateral injection of α-synuclein fibrils, phosphorylated α-synuclein-positive pathology appeared bilaterally (Fig. 3A). In the right hemisphere (injected side), phosphorylated α-synuclein pathology was seen abundantly in dentate gyrus and amygdala, whereas in the left hemisphere no pathology was seen in amygdala and only sparsely in dentate gyrus (Fig. 3A). These results strongly suggest that α-synuclein pathology propagates throughout the brain from the injection site. To understand the spreading pathway of phosphorylated α-synuclein pathology, we investigated in detail the distribution in four coronal sections at 15 months after inoculation (Fig. 3B). Near the injection level (bregma −3.40 mm), abundant phosphorylated α-synuclein pathology was present in substantia nigra, hippocampus, external capsule and entorhinal cortex in right hemisphere, whereas in the left hemisphere, sparser pathology was detected in hippocampus and external capsule (Fig. 3B). By contrast, at the level of 0.02 mm from bregma (3 mm anterior to the injection level), phosphorylated α-synuclein pathology was concentrated in stria terminalis, septal nucleus and cingulate, motor and somatosensory cortex in the right hemisphere. In the left hemisphere, phosphorylated α-synuclein pathology was detected only in septal nucleus (Fig. 3B). These results suggest that phosphorylated α-synuclein pathology does not spread by simple diffusion and the propensity to accumulate phosphorylated α-synuclein seems to differ among brain regions. The time course of spreading of phosphorylated α-synuclein pathology was analysed by immunohistochemistry and summarized in Table 1. Table 1 clearly indicates that induction of phosphorylated α-synuclein pathology in wild-type mice is time- and brain region-dependent. No signs of astrogliosis and inflammation were observed in human α-synuclein fibril-injected mice compared with soluble-human α-synuclein-injected mice at 15 months after injection (Supplementary Fig. 3).

To clarify which α-synuclein species accumulated in the mice, and when, we performed immunoblot analysis with LB509 and anti-mouse synuclein antibodies, which specifically recognize human α-synuclein and mouse α-synuclein, respectively. The antibody specificities are shown in Supplementary Fig. 1B. At a few

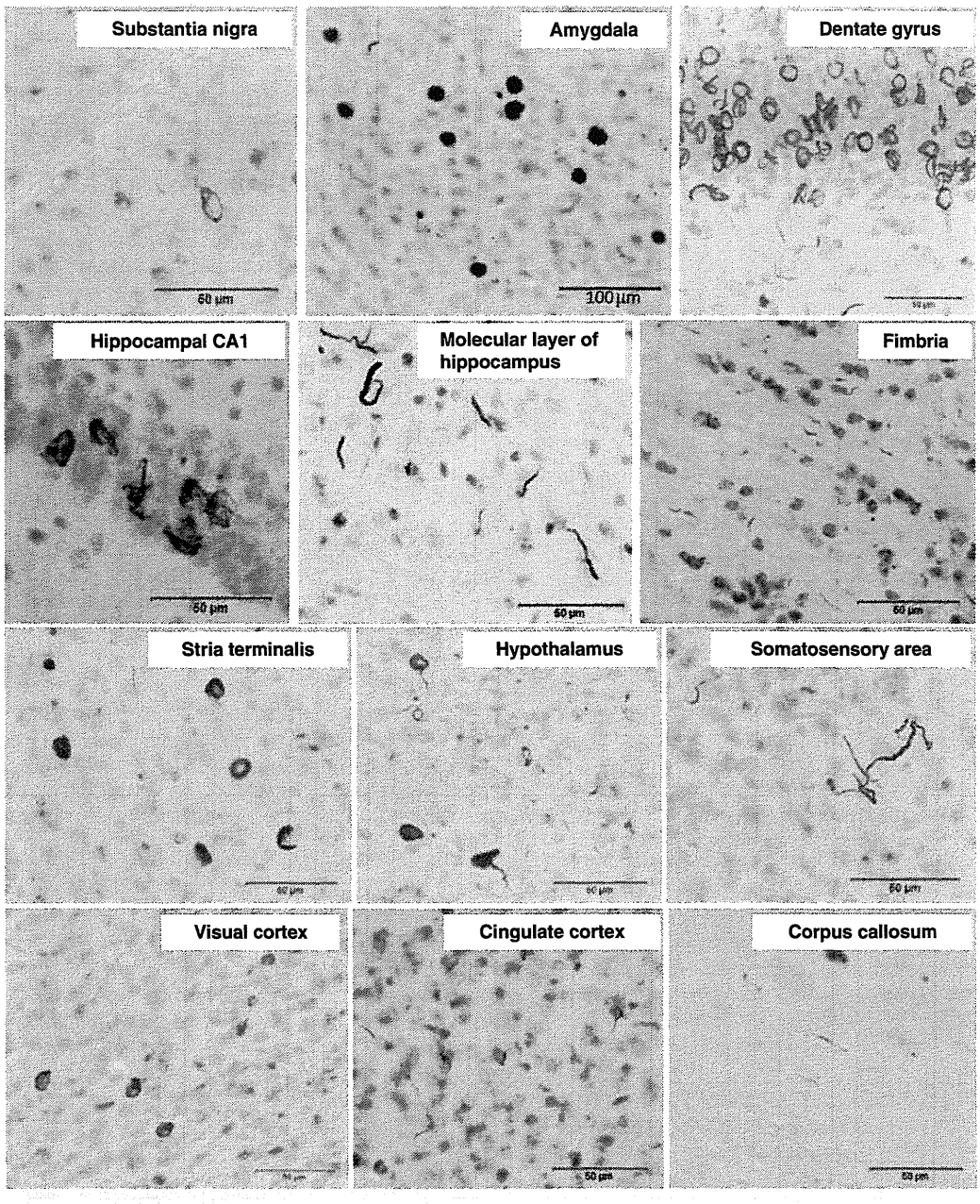

Figure 1 Induction of phosphorylated α-synuclein pathology in wild-type mouse brain injected with human α-synuclein fibrils, observed at 15 months after injection. Sections were immunostained with anti-phosphorylated α-synuclein antibody, 1175. The shapes of phosphorylated α-synuclein-positive structures differed among brain areas. Ring-like and Lewy neurite-like structures were observed in substantia nigra, hippocampus, hypothalamus, somatosensory area, visual cortex, cingulate cortex and corpus callosum, whereas Lewy body- and Lewy neurite-like structures were observed in amygdala and stria terminalis.

hours after injection (Day 0), injected recombinant human α-synuclein fibrils were detected in the sarkosyl-insoluble fraction of the right and left hemispheres by LB509 antibody, suggesting that injected human α-synuclein fibrils in the extracellular space spread quickly throughout the brain. However, at 7 days after injection, the human α-synuclein immunoreactivities had disappeared, and did not reappear at 30 or 90 days after injection (Fig. 4). At 90 days after injection, anti-phosphorylated α-synuclein-positive 15, 20, 30 and 35 kDa bands were detected in the sarkosyl-insoluble fractions. This band pattern is indistinguishable from that of pathological α-synuclein in dementia with Lewy bodies brain (Fig. 4). The 15, 20, 30 and 35 kDa bands correspond to α-synuclein monomer, mono-ubiquitinated α-synuclein, dimer and ubiquitinated dimer, respectively. Most

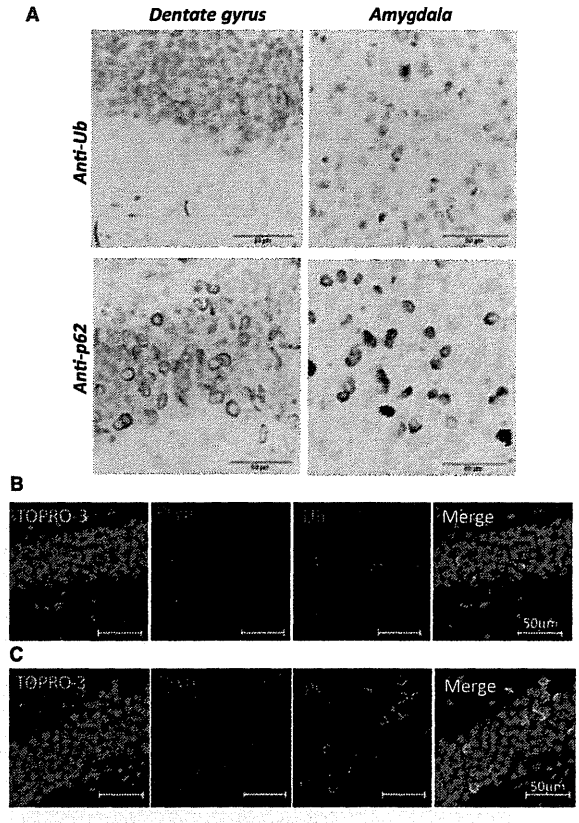

Figure 2 α-Synuclein pathology in fibril-injected mice brain was immunoreactive for ubiquitin (Ub) and p62. **(A)** Staining of dentate gyrus and amygdala of fibril-injected mice at 15 months after injection, using anti-ubiquitin (*upper*) and p62 (*lower*) antibodies. Abundant ubiquitin- and p62-positive pathology can be seen. **(B** and **C)** Double-labelled immunofluorescence of dentate gyrus for phosphorylated α-synuclein (Psyn) and ubiquitin **(B)** or p62 **(C)**. Phosphorylated α-synuclein-positive structures were co-localized with ubiquitin and p62.

interestingly, anti-mouse α-synuclein strongly labelled the sarkosyl-insoluble phosphorylated α-synuclein-positive bands at Day 90, but these were not immunostained with LB509. These results clearly show that endogenous mouse α-synuclein is accumulated as phosphorylated and ubiquitinated forms. Immunohistochemical analysis with anti-tyrosine hydroxylase suggested that dopaminergic neurons are retained in substantia nigra of human α-synuclein fibril-injected mice at 6 months after injection (Fig. 5A and B). However, dramatic loss of the neurotransmitter enkephalin was observed in globus pallidus and amygdala central nucleus, where abundant phosphorylated α-synuclein-positive structures are detected (Fig. 5C and D). These data suggest that neuronal dysfunction occurs without apparent neuronal loss. We also performed behavioural analyses of mice injected with soluble human α-synuclein monomers or human α-synuclein fibrils. However, significant differences were not observed in open field test, wire hang test, rotarod test and Y-maze test (Supplementary Fig. 4) at 6 months after injection.

Next, we tested whether fibrils composed of recombinant mouse α-synuclein can induce α-synuclein pathology more efficiently than those composed of human α-synuclein, because the sequences of human and mouse α-synuclein are slightly different (Supplementary Fig. 5), and there could be a species difference. Mouse α-synuclein complementary DNA was cloned, and the protein was expressed in *Escherichia coli* and purified. Fibrils or soluble mouse α-synuclein were inoculated into substantia nigra of wild-type mouse brains and the pathology was evaluated. Strikingly, all the mice injected with mouse α-synuclein fibrils developed phosphorylated α-synuclein pathology in the injected side of the brain, whereas no pathology was detected in mice injected with soluble mouse α-synuclein (Table 2). The phosphorylated α-synuclein pathologies were basically the same as those of mice injected with human α-synuclein fibrils (data not shown). The efficiency of the induction of phosphorylated α-synuclein pathology by human α-synuclein fibrils was ~90% (Table 2), which is quite high, but slightly lower than that with mouse α-synuclein fibrils, suggesting that there may be a small species difference between mouse and human α-synuclein.

Finally, we tested whether pathological α-synuclein deposited in the brains of patients has similar prion-like properties in brains of wild-type mice. Surprisingly, pathological α-synuclein-enriched fractions also induced phosphorylated α-synuclein-positive pathologies in various areas of brain, including the substantia nigra, amygdala, hippocampus, striatum, hypothalamus, somatosensory area, motor cortex, piriform cortex and superior colliculus (Fig. 6). In brains of these mice, the phosphorylated α-synuclein-positive pathologies mostly resembled Lewy neurite-like structures. Lewy body-like pathology was detected only in amygdala and piriform cortex. The percentage of mice that developed phosphorylated α-synuclein pathology in the injected side of the brains was 50% in the group injected with insoluble phosphorylated α-synuclein of dementia with Lewy bodies brains, which is less than that in mice injected with recombinant α-synuclein fibrils (Table 2). Thus, these results demonstrate that inoculation of either pure synthetic recombinant α-synuclein fibrils or dementia with Lewy bodies brain extracts into wild-type mice can induce Lewy body/neurite-like phosphorylated α-synuclein pathology efficiently and reproducibly. Our results raise an important question, i.e. whether or not α-synuclein fibrils are transmissible among individuals. To test this possibility, we intranasally administered at high concentrarion of abnormal α-synuclein fibrils (preformed recombinant human or mouse α-synuclein fibrils) or the insoluble fraction from dementia with Lewy bodies brain to normal mice. However, no pS129-positive abnormal structures were detected in the brain at 21 months after the final administration (Supplementary Fig. 6), even with highly sensitive immunohistochemical staining, suggesting that the abnormal α-synuclein cannot pass through the nasal mucosa.

Discussion

In this study, we have shown that the inoculation of α-synuclein fibrils made of recombinant α-synuclein or dementia with Lewy bodies brain extracts into wild-type mouse brain is sufficient to

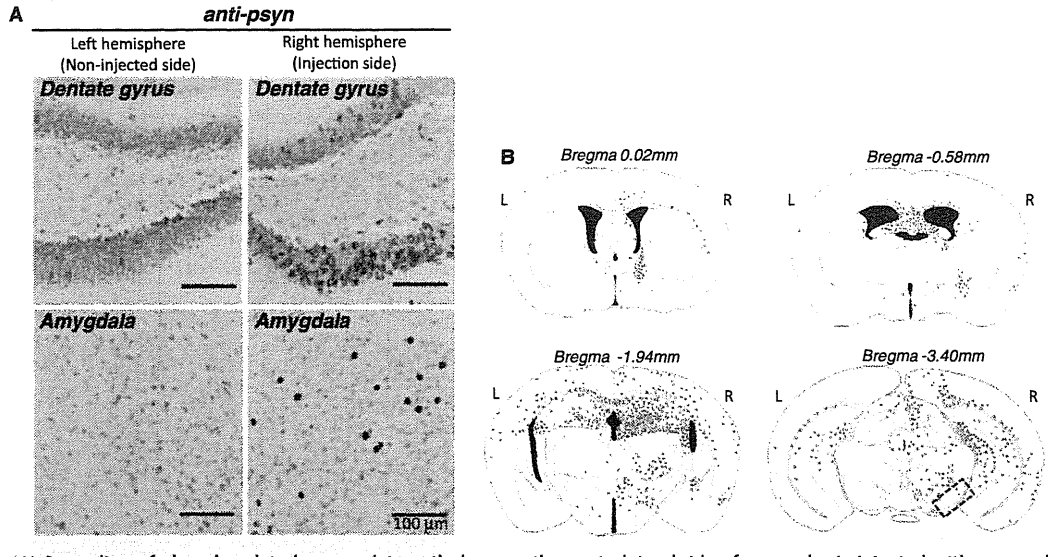

Figure 3 **(A)** Spreading of phosphorylated α-synuclein pathology on the contralateral side of mouse brain injected with α-synuclein fibrils. Staining of dentate gyrus and amygdala in the right hemisphere (injection side) and in the left hemisphere (non-injected side) with anti-phosphorylated α-synuclein (psyn) antibody, 1175, at 15 months after injection. **(B)** Distribution of phosphorylated α-synuclein pathology in human α-synuclein fibril-injected mouse brain at 15 months after injection ($n = 24$). Four coronal sections were stained with phosphorylated α-synuclein antibody, 1175. Red dots indicates Lewy bodies- and Lewy neurites-like pathology. Near the injection level (bregma -3.40 mm), abundant phosphorylated α-synuclein pathology was present in substantia nigra, hippocampus, external capsule, and entorhinal cortex in right hemisphere, whereas in the left hemisphere, sparser pathology was detected in hippocampus and external capsule. At the level of -1.94 mm from bregma, severe phosphorylated α-synuclein pathology was present in hippocampus, amygdala, corpus callosum, hypothalamus and motor, visual, somatosensory, auditory and piriform cortex in the right hemisphere, whereas moderate phosphorylated α-synuclein pathology was observed in corpus callosum, hippocampus, external capsule and motor, somasosensory and auditory cortex in the left hemisphere. At the level of -0.58 mm from bregma, phosphorylated α-synuclein pathology was detected in amygdala, corpus callosum, fimbria, fornix, hypothalamus, striatum and somatosensory and piriform cortex in the right hemisphere, whereas in the left hemisphere, the pathology was present in corpus callosum, fimbria, fornix, hypothalamus and striatum. At the level of 0.02 mm from bregma, phosphorylated α-synuclein pathology was concentrated in stria terminalis, septal nucleus and cingulate, motor and somatosensory cortex in the right hemisphere. In the left hemisphere, phosphorylated α-synuclein pathology was detected only in septal nucleus. Dashed box indicates substantia nigra (injection site). L = left hemisphere of brain; R = right hemisphere.

cause the appearance of Lewy body/neurite-like α-synuclein pathology *in vivo*. Similar work was recently published by Luk *et al.* (2012*a*) but there are important differences between our study and theirs. Luk *et al.* (2012*a*) showed that only inoculation of synthetic mouse α-synuclein fibrils into wild-type mouse brain induced synuclein pathology. In our present study, we inoculated not only fibrils made of recombinant mouse α-synuclein but also ones from human α-synuclein fibrils, and importantly also insoluble α-synuclein from dementia with Lewy bodies brains, into wild-type mouse brain. This is the first report showing efficient induction of α-synuclein pathology by inoculation of material from human brain. Furthermore, our biochemical analyses clearly demonstrate that endogenous mouse α-synuclein is converted into abnormal form and deposited in neurons of the brain through a prion-like mechanism or by seed-dependent aggregation by crossing the species barrier (Fig. 4). Since soluble α-synuclein never induced such pathology (Supplementary Fig. 2), we can conclude that the structural difference between soluble and filamentous forms of α-synuclein, i.e. cross-β structure in the α-synuclein fibrils (Serpell *et al.*, 2000) is critical for the pathogenesis. It has been reported that recombinant α-synuclein fibrils enhance the initiation and progression of α-synuclein pathology in transgenic mice overexpressing mutant α-synuclein (Mougenot *et al.*, 2012; Luk *et al.*, 2012*b*) and wild-type mice (Luk *et al.*, 2012*a*). In those models, α-synuclein pathology appeared at 90 days after inoculation. In our mouse model, abnormal phosphorylated α-synuclein pathology was also detected at 90 days after injection (Fig. 4 and Table 1), suggesting that it takes about this length of time for the formation of abnormal phosphorylated α-synuclein pathology *in vivo* after the seeding procedure. Despite a diffusion of injected exogenous α-synuclein fibrils to the bilateral sides of brain within a few hours after injection (Fig. 4), phosphorylated α-synuclein pathology seems to be initiated in the injected side and to spread from the injected side to the non-injected side in a time-dependent manner (Table 1). Thus, it is reasonable to speculate that exogenous fibrils enter neurons at the injection site as a result of infusion pressure, a temporary high concentration, or some other mechanism, and then the pathological process starts to develop from these cells.

Propagation patterns of pathology in the inoculated mice were basically identical regardless of the species of injected seeds (i.e. recombinant human α-synuclein fibrils, mouse α-synuclein fibrils or

Table 1 Semi-quantitative grading of α-synuclein pathology in mice injected with human α-synuclein fibrils

			Non-injection side (left hemisphere)			Injection side (right hemisphere)		
			Time from injection (days)			Time from injection (days)		
			90	180	450	90	180	450
Bregma	0.02 mm	Stria terminalis	−	−	−	−	+ +	+ + +
		Striatum	−	+	+	+	+ +	+ +
		Cigular cortex	−	−	−	−	+	+
		Septal nucleus	−	−	−	−	+	+
Bregma	−0.58 mm	Corpus callosum	−	−	+	−	−	+ +
		Fornix	−	+	+ +	−	+	+ +
		Hippocampal commissure	−	+	+ +	−	+	+ +
		Amygdala	−	−	−	+	+ + +	+ + +
		Globus pallidus	−	+	+	−	+	+ +
		Striatum	−	−	+	+	+	+
		Somatosensory area	−	−	+	−	+	+
		Insular cortex	−	−	−	+	+	+
Bregma	−1.94 mm	Corpus callosum	−	−	+ +	−	−	+ +
		Hippocampus	−	+	+ + +	+	+ +	+ + +
		Habenular nucleus	−	−	+	−	−	+ + +
		Fimbria	−	+	+ + +	−	+	+ + +
		Amygdala	−	−	−	+ +	+ + +	+ + +
		Hypothalamus	−	−	+	+	+	+ +
		Thalamus	−	−	−	−	−	+
		Visual cortex	−	−	+	−	+	+ +
		Somatosensory area	−	+	+	−	+	+ +
		Auditory cortex	−	−	+	+	+	+ +
		Piriform cortex	−	−	+	+	+	+ +
		External cupsule	−	−	+	−	−	+ +
Bregma	−3.40 mm	Substantia nigra	−	−	−	+	+	+
		Hippocampus	−	+	+ +	+	+ +	+ +
		Superior colliculus	−	+	+	−	+	+ +
		External cupsule	−	−	+	−	−	+
		Visual cortex	−	−	−	+	+	+
		Auditory cortex	+	+	+	+	+ +	+ +
		Entorhinal cortex	−	+	+	+	+ +	+ +

Four coronal sections were stained with anti-phosphorylated α-synuclein antibody at 90, 180 or 450 days after injection. Grading of α-synuclein pathology was performed as follows: −, none; +, slight; + +, moderate; + + +, severe. At 90 days after injection, small amounts of phosphorylated α-synuclein-positive structures were observed in substantia nigra, amygdala, striatum, hypothalamus, hippocampus, and stria terminalis in the right hemisphere of brain (injected side), but very few Lewy neurites were detected in cortex in the left hemisphere. At 180 days post-injection, the amount of phosphorylated α-synuclein-positive pathology was increased and was more widely spread in the right hemisphere, while in the left hemisphere, little phosphorylated α-synuclein pathology was apparent in hypothalamus, hippocampus, striatum or globus pallidus. At 450 days (15 months) after injection, phosphorylated α-synuclein pathology had spread throughout the right hemisphere and the left hemisphere.

dementia with Lewy bodies brain extracts), but extracts of brains with dementia with Lewy bodies showed lower propagation efficiency than recombinant fibrils (Table 2). This relatively low efficiency may be explained by the lesser amount of abnormal α-synuclein contained in the dementia with Lewy bodies brain extracts. Comparison of human α-synuclein fibrils and mouse α-synuclein fibrils indicated that mouse α-synuclein fibrils showed slightly higher efficiency (Table 2). *In vitro* experiments also indicated that mouse α-synuclein fibrils promote fibrillization of the soluble mouse α-synuclein monomer faster than human α-synuclein fibrils (Supplementary Fig. 7). It is well known that prion propagation can cross the species barrier (Prusiner, 1993) and the efficiency of propagation depends on the amino acid sequences of prion proteins. In the case of α-synuclein, mouse α-synuclein and human α-synuclein share 95% amino acid sequence homology (Supplementary Fig. 5), and this may be the reason why endogenous mouse α-synuclein is capable of aggregation by inoculation of human α-synuclein fibrils. Another factor may be that mouse α-synuclein protein has a threonine residue at amino acid position 53 (Supplementary Fig. 5), which is known as an aggregation-prone mutation in familial Parkinson's disease (Polymeropoulos *et al.*, 1997).

Time course analyses of the pathology in these mice (Table 1) showed that at 90 days after injection, phosphorylated α-synuclein pathology was mainly observed near the injection level, but also seen in striatum, amygdala, stria terminalis and dentate gyrus: areas far from the injection site had developed pathology. The striatum and the amygdala central nucleus have projections from substantia nigra, and the stria terminalis serves as a major output pathway of the amygdala (Supplementary Fig. 8). Although the